Drug Design, Development and Therapy

Dovepress
Taylor & Francis Group

Open Access Full Text Article

ORIGINAL RESEARCH

Elucidating the Pharmacological Basis of Xianling Cifang Granules Against Breast Cancer. A Metabolomic Profiling Study

Yang Wang[1,2], Rui Yang[1,3], Youyang Shi[1], Sheng Liu[1,2,4]

[1]Longhua Hospital, Shanghai University of Traditional Chinese Medicine, Shanghai, 200032, People's Republic of China; [2]China Academy of Chinese Medical Sciences, Suzhou, 215100, People's Republic of China; [3]Shanxi Province Cancer Hospital/Shanxi Hospital Afiliated to Cancer Hospital, Chinese Academy of Medical, Sciences/Cancer Hospital Afiliated to Shanxi Medical University, Shanxi, 030013, People's Republic of China; [4]Graduate School, Shanghai University of Traditional Chinese Medicine, Shanghai, 201203, People's Republic of China

Correspondence: Sheng Liu, Shanghai University of Traditional Chinese Medicine, Shanghai, People's Republic of China, Email lslhtcm@163.com

Objective: To analyze the constituents and metabolic products of Xianling Cifang Granules (XLCF) in the serum of mice. The potential targets of XLCF in the treatment of breast cancer (BC) were explored by combining network pharmacology and molecular docking technology.

Methods: Serum was collected from mice following oral administration of XLCF and analyzed using UHPLC-Q Exactive Orbitrap-MS. Absorbed prototype constituents and metabolites were identified by comparing retention times, accurate masses, MS/MS fragments, and isotopic patterns. Network pharmacology predicted potential therapeutic targets, and molecular docking (Autodock/Pymol) validated interactions between key constituents and targets.

Results: Our comprehensive metabolomic profiling elucidates the pharmacological basis of XLCF against BC by identifying its absorbed constituents and their potential therapeutic links. It identified 122 prototype constituents of XLCF entering the systemic circulation. Icaritin (a metabolite derived from *Epimedium brevicornu Maxim*) was identified as a pivotal constituent due to its high bioavailability and established anti-BC activity, specifically inducing redox-mediated apoptosis via the SIRT6/NF-κB pathway and modulating the immunosuppressive microenvironment in triple-negative breast cancer (TNBC). Additionally, 62 serum metabolites exhibited significant alterations post-XLCF treatment, indicative of metabolic reprogramming involving carboxylation, hydroxylation, glucuronidation, and sulfation. Network pharmacology implicated inflammation and cellular metabolism pathways in the therapeutic effects of XLCF. Molecular docking confirmed that Icaritin, as the principal bioactive component, formed stable interactions with core targets ADORA1, AKR1B1, and ADORA3.

Conclusion: This integrated approach delineates the anti-BC mechanism of XLCF, 122 absorbed constituents (with Icaritin as key) and 62 altered metabolites drive systemic metabolic reprogramming, acting through ADORA1, AKR1B1 and ADORA3 targets to modulate critical pathways. These findings provide robust pharmacological evidence supporting the clinical application of XLCF against BC and demonstrate the value of combining metabolomics with target prediction for Traditional Chinese Medicine (TCM) research. Experimental validation of the identified targets is warranted.

Keywords: Xianling Cifang granules, UHPLC-Q exactive Orbitrap-MS, prototypes, metabolites, network pharmacology

Introduction

Breast cancer (BC) poses a significant threat to the life and health of women worldwide, ranking among the top diseases in terms of incidence and mortality. Clinically, BC often exhibits heterogeneity and has a propensity to metastasize to organs such as the lungs, liver, bones and brain.[1] Currently, the lack of specific therapeutic targets means that traditional chemotherapy still plays a dominant role in its treatment.[2,3] However, the efficacy of chemotherapy is often suboptimal, and it frequently is confronted with barriers including severe side effects. Although immune checkpoint inhibitors (ICIs) have demonstrated remarkable therapeutic potential in recent years, their effectiveness is limited to PD-L1-positive

Received: 17 April 2025
Accepted: 9 September 2025
Published: 13 September 2025

patient populations, which restricts their widespread application in BC treatment. Therefore, there is an urgent need to identify therapeutic drugs and strategies that can effectively inhibit BC with minimal side effects and low drug resistance rates, as well as to develop methods to address the limitations of immunotherapy.

Traditional Chinese Medicine (TCM) posits that tumors are often caused by phlegm and toxin pathogenic factors. Our research team, through clinical practice, has identified 5 TCM herbs with the effects of dispersing lumps and detoxifying, which are formulated into "Xianling Cifang Granules" (XLCF). The formula primarily uses *Iphigenia indica Kunth* and *Polistes mandarinus Saussure* as the sovereign drugs, both of which have mighty anti-cancer and dispersing effects, embodying the concept of "fighting poison with poison". *Iphigenia indica Kunth* was first documented in the "Ben Cao Shi Yi" during the Tang Dynasty in China and is a relatively commonly used TCM. Clinically, it is applied in the intervention of malignant neoplasms, including but not limited to BC, as well as gout, demonstrating significant therapeutic value.[4] Modern pharmacological studies have shown that *Iphigenia indica Kunth* contains colchicine and its derivative colchicine amide, which exhibit inhibitory effects on various animal transplantable tumors. *Polistes mandarinus Saussure* is described in the "Shen Nong Ben Cao Jing" as follows: it has a bitter and salty taste, is neutral in nature, and is toxic. It is primarily used to treat convulsions, spasms, chills and fever, pathogenic factors, manic disorders, ghostly influences, and toxic substances such as intestinal hemorrhoids. Additionally, *Polistes mandarinus Saussure* belongs to the Yangming Stomach Meridian, endowing it with wind-dispelling and detoxifying properties. It can reach from the top of the head to the lower abdomen, acting on both the exterior and interior of the body, as well as on both the organs and bowels. It regulates the triple burner (Sanjiao) without stagnation and harmonizes the flow of Qi smoothly. *Curcuma zedoaria* is used as the ministerial drug to break up blood stasis and eliminate accumulations, working together to reduce tumors and disperse lumps. Furthermore, *Epimedium brevicornu Maxim* and *Fructus Alebiae* are used as adjuvant and envoy drugs, respectively, to soothe the liver and regulate qi, as well as to tonify the kidney and strengthen the bones, ensuring that the entire formula expels pathogenic factors without harming the body's vital energy. Consequently, it could exert the effects of dispersing lumps and detoxifying for better results.

In the preliminary clinical research of our team, a prospective follow-up study of two years involving a total of 80 cases was designed to investigate the clinical efficacy of XLCF in preventing postoperative recurrence and metastasis of BC. The results demonstrated that XLCF suppressed the metastasis of BC. Additionally, its efficacy was superior to that of TCM based on the principles of tonifying qi and nourishing yin, as well as regulating the Chong and Ren meridians. Experimental studies in vivo had confirmed that XLCF protected the soundness of the vasculature and impeded the generation of a pre-metastatic niche by downregulating the transcription of VEGF, Angpt2, ultimately inhibiting the incidence of tumor spread to the lungs. Cellular experiments in vitro studies have elucidated that XLCF can suppress the invasion and metastatic capabilities of BC cells. Network pharmacological analysis indicated that the anti-BC effects of XLCF may be linked to downregulating TGFβ, enhancing apoptosis, and preventing angiogenesis.[5,6] Current research had confirmed that XLCF could suppress BC metastasis by protecting the integrity of lung blood vessels.[7–9] These results offer substantial theoretical support for the application of XLCF in treating BC.

However, to gain a more comprehensive insighting of its working principles and to promote its further development and utilization, there is a need for comprehensive investigation on the chemical components and metabolites of XLF in mice serum.

In the field of TCM pharmacology, the study of serum metabolite profiles holds great importance. Metabolomics, as an emerging discipline, focuses on the holistic effects of exogenous substances on organisms and investigates the systemic impact of drugs on the metabolic network within the body. Compared to other "omics" approaches, metabolomics studies the end products of gene and protein interactions, making it more reflective of the organism's ultimate response to drugs. Therefore, the research methods of metabolomics align with the holistic concept of TCM in treating diseases, aiding in elucidating the therapeutic mechanisms and efficacy of TCM, and providing a basis for rational drug design and personalized medicine.

In this study, we employed advanced analytical techniques such as UHPLC-Q Exactive Orbitrap-MS, which offers unparalleled resolution and mass accuracy, enabling precise identification and quantification of complex TCM components and their metabolites. Using this technology, a thorough analysis of the chemical components and metabolites of XLCF in mouse serum was conducted by us, thereby addressing the lack of in vivo metabolite data in previous XLCF

studies.[10,11] This advanced analytical tool not only facilitates rapid screening, metabolic profiling, and target prediction but also accelerates the discovery and development of novel therapeutic agents from TCM. By applying these techniques, we can systematically investigate the chemical composition of XLCF and its metabolic processes in vivo, revealing its modes of functioning and providing empirical data for the advancement of innovative medications. In addition, we combined network pharmacology and molecular docking to explore its therapeutic mechanism and ultimately contribute to the treatment of BC.

Materials and Methods

Reagents and Materials

XLCF Granules (5g/bag, manufactured by Shanghai Wanshicheng Pharmaceutical Co., Ltd.) were purchased from the Traditional Chinese Medicine Pharmacy of Longhua Hospital affiliated to Shanghai University of Traditional Chinese Medicine. MS-grade methanol, acetonitrile, and formic acid were purchased from Thermo Fisher Scientific (Waltham, MA, USA). Ultrapure deionized water was sourced from Unique-R20 Water Purification Systems (Xiamen, China). The ultrasound was purchased from Shanghai Kedao Ultrasonic Instrument Co.,Ltd. (Shanghai, China). The grinding instrument was purchased from Shanghai Wanbai Biological (Shanghai, China). The anticoagulant tube was purchased from Becton, Dickinson and Company (Shanghai, China). The centrifuge was purchased from Beckman Coulter Ltd. (Waltham, MA, USA).

Sample Preparation

We dispensed approximately 100 μL of serum sample into a 1.5 mL centrifuge tube; added 900 μL of water (containing mixed internal standards at 4 μg/mL), vortexed for 1 minute; extracted by ultrasound in an ice-water bath for 60 minutes, and allowed to stand at −40°C for 30 minutes; centrifuged for 10 minutes at 12,000 rpm and 4°C; after diluting 10 times with water (containing mixed internal standards at 4 μg/mL), 200 μL of the diluted solution was loaded into an LC-MS injection vial lined with an insert tube for analysis.

Reference Substances

The LuMet-TCM reference substances database was developed by Luming Biotech Co., Ltd., based in Shanghai, China.

Animals

All animal experiments adhered to protocols sanctioned by the Animal Protection and Use Committee of Shanghai University of Traditional Chinese Medicine (Permit No.: LHERAW-25020). Ten 5-week-old female SPF-grade BALB/c mice were procured from Shanghai Slack Experimental Animal Co., Ltd. (Production License No.: SCXK (Hu) 2018–0004) and kept in the Experimental Animal Center of Longhua Hospital, Shanghai University of Traditional Chinese Medicine. The housing conditions were maintained at (22±2) °C, 50–60% relative humidity, and a 12-hour light/dark cycle, allowing the mice free access to food and water. After a one-week acclimation period, the experiments began. Animal welfare was ensured in accordance with the "Guidelines for the Ethical Review of Welfare for Laboratory Animals" (GB/T 35892–2018).

Preparation of Mice Plasma and Lung Tissue

Following the acclimatization period, mice were randomly assigned to either the treatment or control group, with 5 mice per group. The control group received normal saline by gavage, while the treatment group received XLCF Granule solution by gavage. Gavage was administered at a volume of 0.25 mL each time, morning and evening, for 3 consecutive days. Food was withheld for 12 hours before the last gavage administration (water was not restricted). One hour after the final administration, the mice in both the treatment and control groups were anesthetized with 10% chloral hydrate. Blood was collected from eyeballs at 0.5h, 1h, 2h.

LC-MS/MS Analysis

An ACQUITY UPLC I-Class Plus system (Waters Corporation, Milford, USA) coupled with a Q-Exactive mass spectrometer equipped with a heated electrospray ionization (ESI) source (Thermo Fisher Scientific, Waltham, MA, USA) was employed for metabolomic profiling in both positive and negative ESI modes. An ACQUITY UPLC HSS T3 column (1.8 μm, 2.1×100 mm) was used for separation. The binary gradient elution system, consisting of (A) water with 0.1% formic acid (v/v) and (B) acetonitrile with 0.1% formic acid (v/v), was applied with the following gradient: 0.01 min, 5% B; 2 min, 5% B; 4 min, 30% B; 8 min, 50% B; 10 min, 80% B; 14 min, 100% B; 15 min, 100% B; 15.1 min, 5% B; 16 min, 5% B. The flow rate was maintained at 0.35 mL/min, and the column temperature was set at 45°C. Samples were kept at 4°C during analysis, with an injection volume of 5 μL.

Data Preprocessing and Statistical Analysis

LC-MS data were processed using Progenesis QI V2.3 (Nonlinear Dynamics, UK) for baseline filtering, peak alignment, and normalization. Compound identification relied on accurate mass (m/z), secondary fragments, and isotopic distribution, referencing the LuMet-TCM, Animal_DB, and Herb databases. Tolerances were set at 5 ppm for precursors and 10 ppm for products.

After consolidating and de-weighting the substances detected in both ion modes, the total relative peak area of metabolites was normalized to 100% to create a data matrix for qualitative and quantitative analysis. This matrix, containing all extracted information, supports subsequent analyses. For each identified TCM ingredient and blood component, EICs and MS2 spectra with annotated fragment structures were generated. Pie charts were also created to show the distribution of TCM components by chemical classification and content.

Network Pharmacology and Molecular Docking

Screening Targets for LH Active Ingredients

High-resolution mass spectrometry platforms were utilized to detect the constituents of medicinal materials, or alternatively, the components and their corresponding SMILES and InChiKeys were retrieved from the HERB database based on the name of the herbs. The pharmacological properties of the constituents, including pharmacodynamic and bioactivity profiles, physicochemical properties (such as solubility and logP), and pharmacokinetic parameters (absorption, distribution, metabolism, and excretion), were predicted using the SwissADME website. The screening criteria included compliance with three or more of the Lipinski, Ghose, Veber, Egan, and Muegge rules for drug-likeness, indicated by a "yes" response, which suggests good druggability of the compounds; and a "high" gastrointestinal absorption (GI absorption) result, indicating good bioavailability. Compounds that met both of these criteria were considered as active components.

Potential targets of the active components were predicted using the SwissTargetPrediction website, with the top 20 targets being designated as potential therapeutic targets. All targets were compiled and entered into the UniProt database (https://www.uniprot.org) to correct the gene names of the drug targets, thereby standardizing the protein target information.

Screening Targets Associated with Breast Cancer

Search using the terms "Breast Cancer" to identify targets related to BC in the GeneCards (https://www.genecards.org/).

Target Pathway Annotation Analysis

In the Gene Ontology (GO) database (http://www.geneontology.org) and Kyoto Encyclopedia of Genes and Genomes (KEGG) database (https://www.genome.jp/kegg/), with human genes as the scope, $p < 0.05$ for screening value, obtain the corresponding data.

Analysis of Protein Interaction Networks

The species/closely related species (blast e-value:1e-5) were selected in the STRING (https://string-db.org/) database to analyze the intersection target proteins, obtain the interaction relationship, select the top 25 proteins in terms of connectivity, recalculate the connectivity of these proteins and draw the network diagram.

Construction of an Active Ingredient-Breast Cancer Target-Pathway Network

The action targets of the active components of XLCF regulating BC were introduced into Cytoscape 3.10.2, and the network diagram of "components-targets-pathways" was constructed. The "Tools analysis network" in Cytoscape was used to analyze the complex relationships between active ingredients and targets and the disease of XLCF, visualize the component regulatory disease date network, and predict the potential therapeutic targets of XLCF for BC.

Potential Active Ingredients/Key Targets, and Molecular Docking Validation

This docking was carried out using Autodock vina2.1.6. After the docking was completed, the conformation with the best binding energy and the most repeated binding conformations was selected as the output result, and the results were imported into Pymol 3.1 and Discovery Studio 2019 respectively for visual analysis.

Results

Identification of Chemical Components in XLCF in vitro

The chemical components of XLCF were characterized by LC-MS, as detailed in Figure 1. The compounds were provisionally identified. Figure 2 illustrates the UHPLC-MS basepeak chromatogram (BPC) profiles of XLCF in two modes. For compound identification, XLCF was compared against the reference substances database (LuMet-TCM) based on accurate mass, fragment ions, and isotopic patterns. Utilizing this identification approach, a total of 913 chemical compounds in XLCF were identified, encompassing flavonoids, terpenes, carbohydrates and glycosides, amino acids, peptides and derivatives, and other compounds. All 913 compounds were identified by comparison with reference standards, and detailed information is provided in Supplementary Table 1. Figure 3 illustrates the classification and

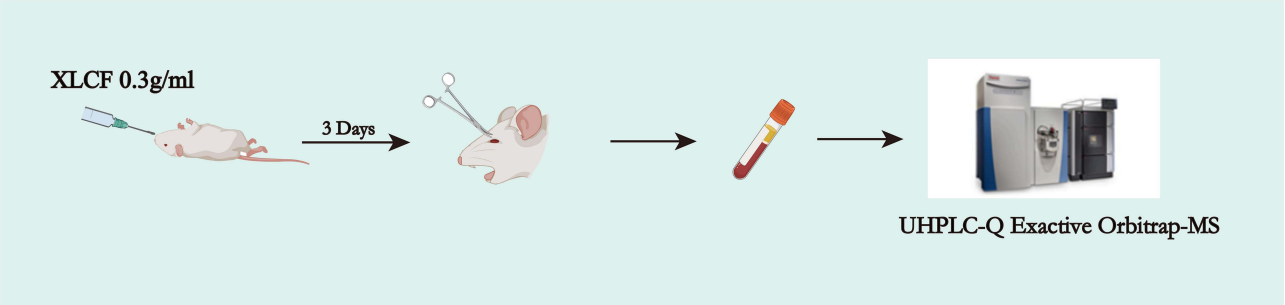

Figure 1 The dosing regimen for the identification of serum and metabolic products of XLCF in mice.

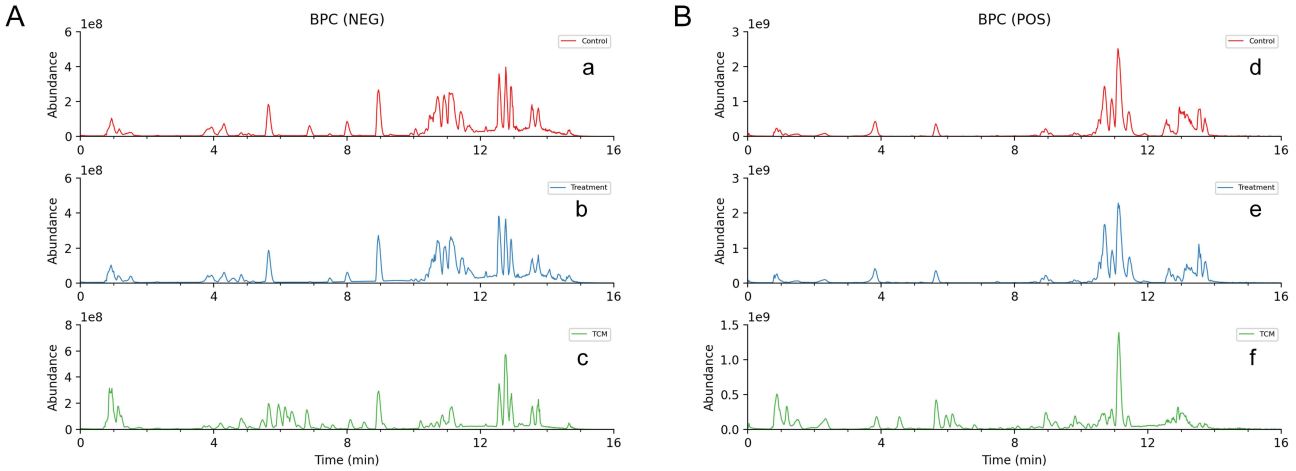

Figure 2 Characterization of chemical constituents in mice serum (**A** and **B**). Base-peak chromatogram (BPC) of XLCF obtained by LC-MS analysis. (**A**) Negative-ion scan (a: control serum, b: XLCF-containing serum, c: XLCF sample). (**B**) Positive-ion scan (d: control serum, e: XLCF-containing serum, f: XLCF sample).

https://doi.org/10.2147/DDDT.S530516

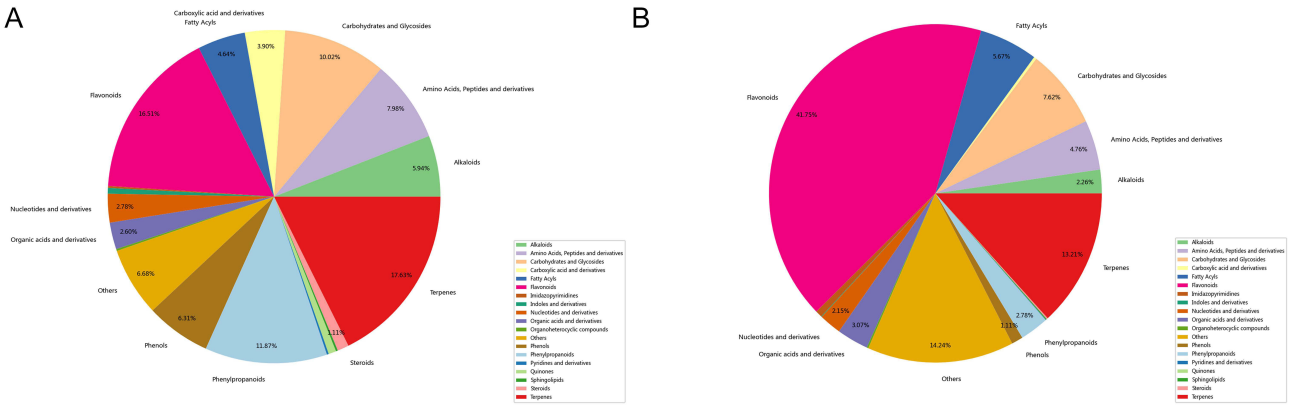

Figure 3 Classification of Ingredients in Traditional Chinese Medicine. (**A**) Distribution Chart of Classified Quantities of Ingredients in Traditional Chinese Medicine. (**B**) Distribution Chart of Classified Contents of Ingredients in Traditional Chinese Medicine.

abundance distribution of the chemical components in the TCM. The top five categories by quantity are Terpenoids (17.63%), Flavonoids (16.51%), Phenylpropanoids (11.87%), Carbohydrates and Glycosides (10.02%), and Amino acids, Peptides and derivatives (7.98%). In terms of abundance, the top five categories are Flavonoids (41.75%), Terpenoids (13.21%), Carbohydrates and Glycosides (7.62%), Fatty acyls (5.67%), and Amino acids, Peptides and derivatives (4.76%).

Terpenoids

A total of 95 Terpenoids were identified in XLCF through database comparison, including asiaticoside, macranthoidin A, codonolactone, xanthatin, furanodienone, dihydroactinidiolide, and others. Figure 4a and b present the extracted ion chromatograms (EIC) for asiaticoside and macranthoidin A, respectively, alongside their MS/MS spectra juxtaposed with the LuMet-TCM database. Literature evidence indicates that asiaticoside significantly inhibits BC proliferation.[12] Mechanistic investigations further reveal that its anti-tumor effects are mediated through the suppression of inflammatory pathways.[13] Take snow asiaticoside as an example, in the negative ion mode, a quasi-molecular ion peak with an *m/z* value of 1003.5130 was observed at a retention time of 5.83 min, corresponding to a predicted molecular formula of $C_{48}H_{78}O_{19}$. The primary fragment ions exhibited *m/z* values of 101.0245 and 487.3432, with the molecular ion peak appearing at 1003.5164. Upon comparison with the database, the identification of *m/z* values 161.0456, 247.0826, 367.1205, 469.1562, and 957.5071 confirmed the compound as asiaticoside. Figure 4a shows the relevant data.

Flavonoid

By comparing with the database, 89 Flavonoid components were identified in XLCF, ranking second in proportion. These include 2"-O-Rhamnosylicariside II, Baohuoside V, baicalin, sophoflavescenol, trifolin, and others. Figure 4c and d present the extracted ion chromatograms (EIC) of 2"-O-Rhamnosylicariside II and Baohuoside V, respectively, along with their MS/MS spectra compared with the LuMet-TCM database. Literature indicates that Baohuoside V, as the main active component in Epimedium, can inhibit the proliferation of BC cells in a dose-dependent manner.[14] Taking compound 2 as a case in point with an *m/z* of 661.2484 was detected at a retention time of 8.52 min, with a predicted molecular formula of $C_{33}H_{40}O_{14}$. The main fragment ion peaks observed were *m/z* 85.0289, 129.0547, 313.0707, 369.1335, 479.1705, and 515.1912. After database comparison, the *m/z* values 379.0810, 405.0971, 411.1443, 423.1073, and 435.1444 further confirmed the compound as 2"-O-Rhamnosylicariside II. The matching score and fragmentation score were 59.5 and 62.8, respectively, and a mass error as low as −1.06 ppm validated the precision of the analysis. The EIC spectrum, the molecular masses of the secondary fragments, and the structural layout of 2"-O-Rhamnosylicariside II are illustrated in Figure 4c.

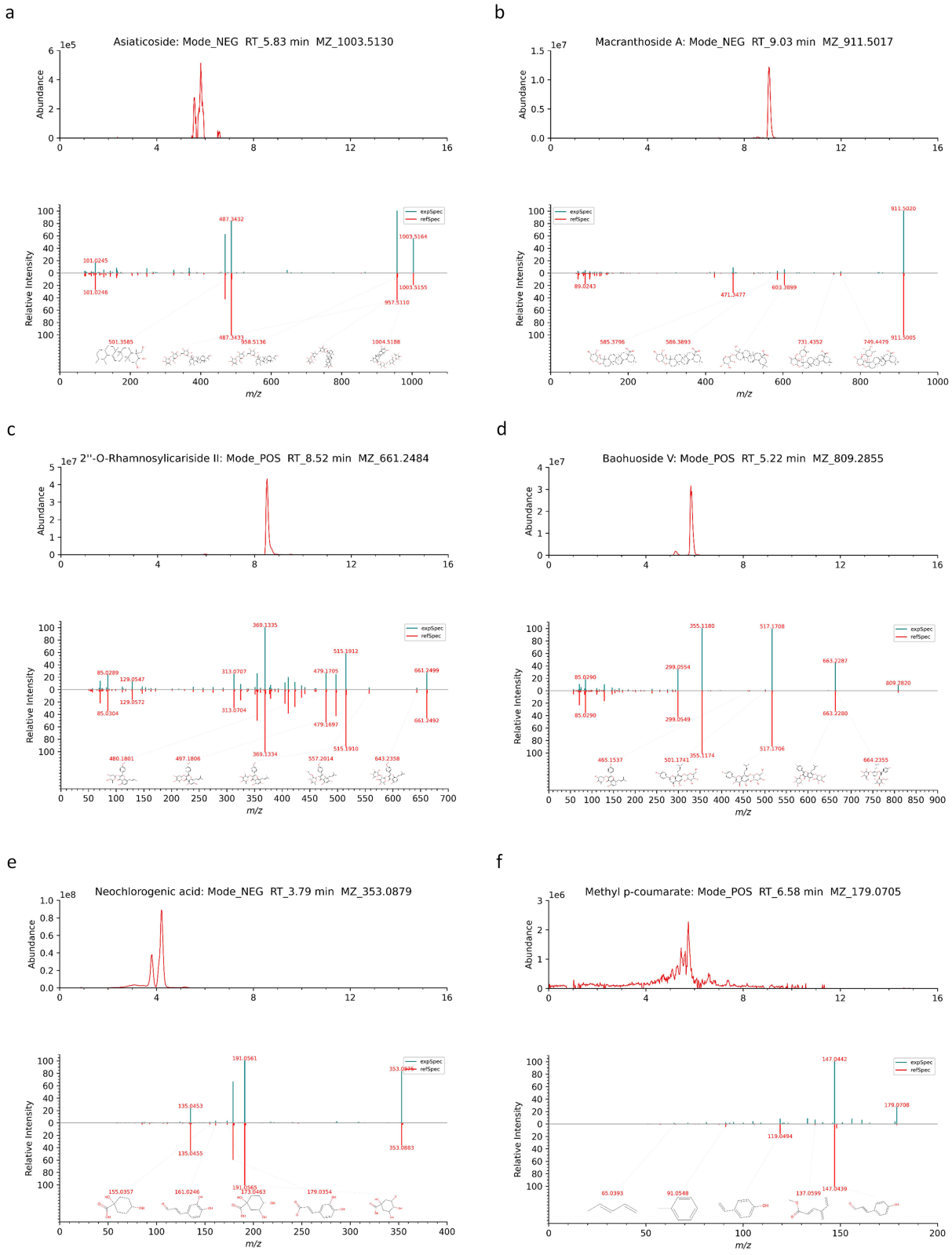

Figure 4 Continued.

https://doi.org/10.2147/DDDT.S530516

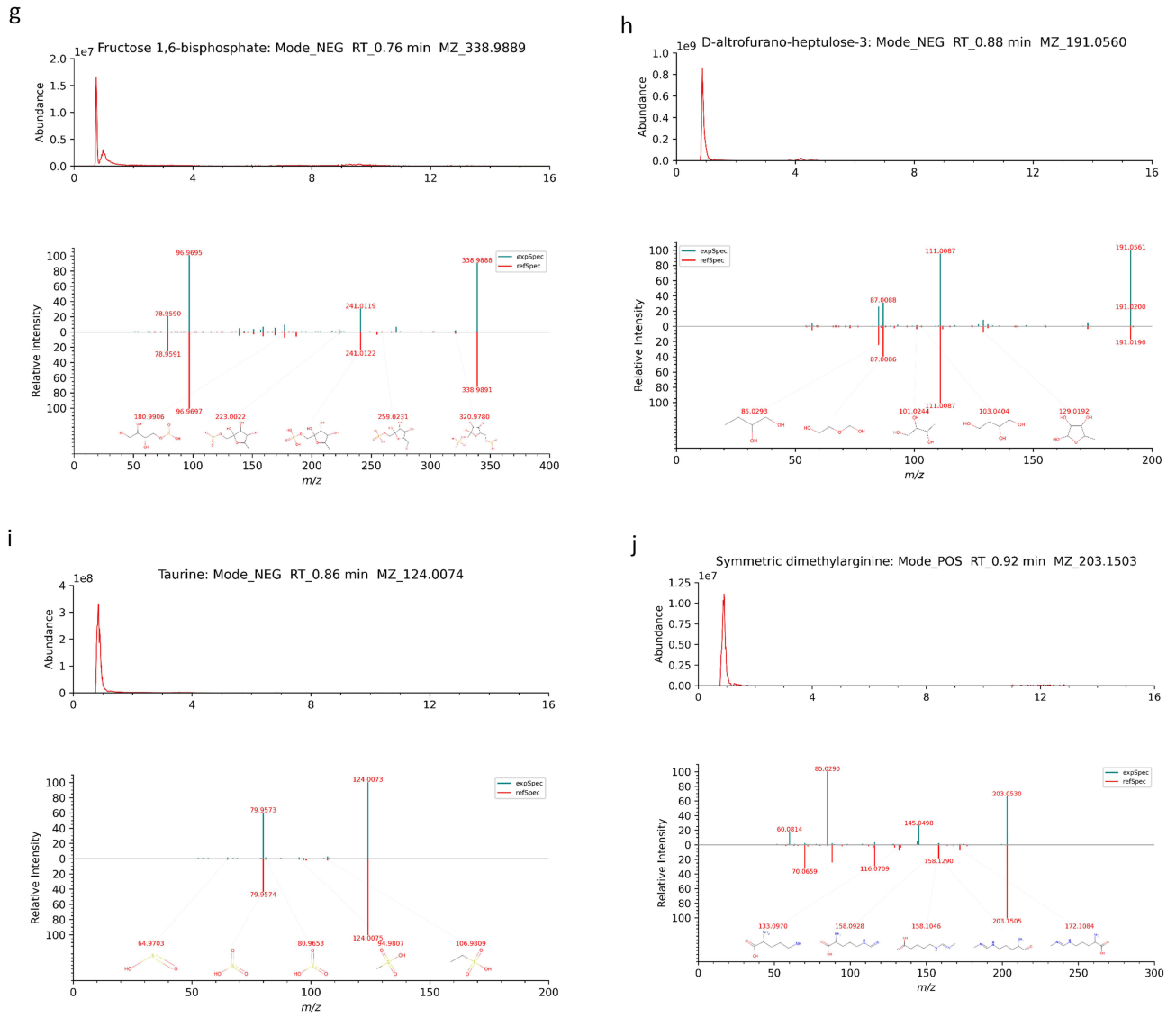

Figure 4 EICs of each chemical and MS/MS spectrum compared with databases. (**a**) Asiaticoside. (**b**) Macranthoside A. (**c**) 2"-O-Rhamnosylicariside II. (**d**) Baohuoside V. (**e**) Neochlorogenic acid. (**f**) Methyl p-coumarate. (**g**) Fructose 1,6-bisphosphate. (**h**) D-altrofurano-heptulose-3. (**i**) Taurine. (**j**) Symmetric dimethylarginine.

Phenylpropanoids

In the active components of XLCF, a total of 64 Phenylpropanoids were identified, including neochlorogenic acid, methyl p-coumarate, sinapaldehyde, coniferaldehyde, dihydrocoumarin, and others. Figure 4e and f display the EIC of neochlorogenic acid and methyl p-coumarate. Literature evidence identifies neochlorogenic acid as a dominant compound in cultivated plants, which exhibit significant in vitro anti-tumor activity against BC.[15] So take it as an example, compound 137 shows a quasi-molecular ion peak with an *m/z* of 353.0879 at a retention time of 3.79 min in negative ion mode, with a predicted molecular formula of $C_{16}H_{18}O_9$. The main fragment ion peaks observed were *m/z* 135.0453 and 191.0561. After database comparison, the *m/z* values 135.0453 and 191.0561 confirmed the compound as neochlorogenic acid. Figure 4e depicts the EIC, the mass values of the secondary fragments, and the structural configuration of neochlorogenic acid.

Carbohydrates and Glycosides

In the active components of XLCF, 54 Carbohydrates and Glycosides were identified, including fructose 1,6-bisphosphate, D-altrofurano-heptulose-3, gluconic acid, glucose 6-phosphate, phaseoloidin, and others. Figure 4g and h present the EIC and MS/MS spectra of fructose 1,6-bisphosphate and D-altrofurano-heptulose-3, respectively. Consider

compound 255 as an example, in negative ion mode, a quasi-molecular ion peak with an *m/z* of 338.9889 was detected and the peak appeared with a retention time of 0.76 min, with a predicted molecular formula of $C_6H_{12}O_7$. The main fragment ion peaks observed were *m/z* 78.9590, 96.9695, and 241.0119. After database comparison, the *m/z* values 59.0138, 75.0087, 87.0088, 99.0088, 129.0193, 159.0297, 177.0405, 195.019, and 195.0509 suggested that the compound is fructose 1,6-bisphosphate. The specific ion chromatogram, molecular weights of the secondary fragments, and structure of fructose 1,6-bisphosphate are illustrated in Figure 4g.

Amino Acids, Peptides and Derivatives

Through comprehensive analysis and identification, a total of 43 components in XLCF were detected as Amino acids, Peptides and derivatives. These include taurine, symmetric dimethylarginine, valylleucine, citrulline, gamma-glutamylleucine, gamma-Glu-Phe, and others. Figure 4i and j present the EIC and MS/MS spectra of Taurine and Symmetric dimethylarginine. Studies have documented that overexpression of taurine-secreted proteins is associated with BC, suggesting their potential as therapeutic targets for anti-cancer treatment.[16] Taking compound 190 as an example, in negative ion mode, a prominent molecular ion peak with an *m/z* of 124.0074 was detected at a retention time of 0.86 min, with a predicted molecular formula of $C_2H_7NO_3S$. The main fragment ion peaks observed were *m/z* 79.9573 and 124.0073, which are consistent with the literature,[17] suggesting that the compound is taurine. Figure 4i illustrated clearly.

Identification of Absorbed XLCF Components in Mouse Serum

Plasma was collected from mice at multiple time points after oral administration of XLCF over a 3-day period. Samples collected at various time points were combined to create the dosed serum for subsequent analysis. In order to identify the absorbable components of XLCF, a UHPLC-Q Exactive Orbitrap-MS method was initially developed for screening purposes. A total of 122 prototype constituents were identified within the XLCF-dosed serum by comparing its data with that of blank serum and conducting a qualitative analysis of the original XLCF ingredients in vitro. These constituents encompassed a range of compounds, such as Terpenes, Organic acids and derivatives, Nucleotides and derivatives, Imidazopyrimidines, Flavonoids, Carbohydrates and Glycosides, as well as other compounds that have yet to be classified into specific categories. Among these, Terpenes and Flavonoids were the most prevalent categories. The identified absorbed components are detailed in Table 1, which presents the theoretical *m/z* values, measured *m/z* values, fragment ions, and molecular formulas. Notably, the mass errors were all below 5 ppm. Among the identified components, Icariin (Figure 5a), 2"-O-rhamnosylicariside II (Figure 5b), and zederone (Figure 5c) exhibit relatively high relative abundances and demonstrate potential pharmacological activity in subsequent functional validation studies. Below, we will provide a detailed discussion on the structural characteristics, metabolic pathways, and mechanisms of action of these three monomers.

Icariin

In mouse serum, the extracted Electron Capture Ionization (ECI) chromatogram of Icariin in positive ion mode demonstrated a signal at *m/z* 677.2435 with a retention time of 6.13 minutes. The main fragment ion peaks were at *m/z* 313.0708, 369.1337, 531.1862, and 677.2408. The scores and fragmentation scores were 65.6 and 86.3, respectively, reflecting the accuracy of the spectrum. Experimental studies have indicated that Icaritin can induce redox-mediated apoptosis via the SIRT6/NF-κB signaling pathway, while also suppressing metastasis and modulating the immunosuppressive tumor microenvironment in TNBC, indicating that Icaritin could be a viable therapeutic option for TNBC.[18]

2"-O-Rhamnosylicariside II

The detection results in the serum showed that 2"-O-Rhamnosylicariside II exhibited a peak at *m/z* 661.2484 at a retention time of 8.52 minutes, which was particularly prominent in the TCM group samples. In the control spectrum, the main fragment ion peaks were observed at *m/z* 85.0289, 129.0547, 313.0707, 369.1335, 479.1705, 515.1912, and 661.2499. The scores and fragmentation scores were 59.5 and 62.8, respectively, with a mass error as low as −1.06 ppm, further validating the precision of the analysis. Studies have found that Icariin is a compound with significant pharmacological effects that is rarely found in nature. Utilizing a whole-cell catalyzed biotransformation method

https://doi.org/10.2147/DDDT.S530516

Table 1 Identification of the Chemical Constituents of XLCF in Serum

No.	Adducts	Formula	Mass Error (ppm)	Fragment Ions	theoretical *m/z*	*m/z*	Rt /min	Ion mode
1	M+Na	$C_{32}H_{34}O_{18}$	−1.15	377.0999, 553.1324, 729.1642	729.1638	729.1629	5.01	POS
2	M+H, M+K, M+Na	$C_{33}H_{40}O_{14}$	−1.06	369.1335, 379.0810, 405.0971, 411.1443, 423.1073, 435.1444, 479.1705, 497.1805, 515.1912, 661.2499	661.2491	661.2484	8.52	POS
3	M+Na, M+K, M+H, M+H-H_2O	$C_{15}H_{18}O_3$	−0.83	269.115	269.1148	269.1146	9.82	POS
4	M+H, M+Na	$C_{10}H_7NO_4$	0.69	146.0606, 149.0236, 178.0502, 188.0705, 206.0451	206.0448	206.0449	3.52	POS
5	M-H	$C_{10}H_{12}O_7S$	0.92	103.9201, 137.0244, 180.0424, 187.0063, 190.0533, 195.0328, 195.0661, 216.9817, 274.9868, 275.0230	275.0231	275.0234	4.05	NEG
6	M-H	$C_{15}H_{14}O6$	1.04	109.0295, 125.0243, 179.0353, 203.0711, 205.0506, 245.0818, 289.0714	289.0718	289.0721	4.22	NEG
7	M-H	$C_{17}H_{14}O_7$	0.74	299.0196, 314.0433, 328.2207, 329.0668	329.0667	329.0669	7.09	NEG
8	M+Na	$C_{24}H_{28}O_{12}$	3.99	299.0552, 355.1178, 531.15	531.1472	531.1493	5.47	POS
9	M-H_2O-H, M-H	$C_7H_{14}O_7$	−0.63	85.0295, 87.0088, 111.0087, 129.0192, 191.02, 191.0561	191.0561	191.056	0.88	NEG
10	M-H	$C_9H_6O_7S$	0.57	177.0192, 189.1129, 190.0507, 256.9765	256.9761	256.9763	4.24	NEG
11	M+Na	$C_{10}H_{12}N_4O_4$	0.68	159.0279, 230.1393, 258.1337	275.0751	275.0752	1.7	POS
12	M-H	$C_{10}H_{13}N_5O_5$	0.5	117.0193, 121.0443, 133.0153, 150.0421, 282.0843	282.0844	282.0845	1.51	NEG
13	M-H	$C_5H_4N_4O_2$	−0.34	108.0203, 151.026	151.0261	151.0261	1.24	NEG
14	M-H	$C_{27}H_{28}O_{12}$	0.51	113.0246, 175.0254, 297.0396, 309.0413, 352.0941, 367.1187, 543.1461	543.1508	543.1511	8.45	NEG
15	M-H, 2M-H	$C_{10}H_{12}N_4O_5$	0.32	135.0312, 267.0735	267.0735	267.0736	1.51	NEG
16	M+H	$C_{26}H_{26}O_{12}$	−0.91	299.0552, 355.1179, 531.1504	531.1497	531.1492	6.46	POS
17	M-H	$C_{27}H_{26}O_{18}$	−0.81	112.9857, 285.0406, 461.0732, 637.1063	637.1046	637.1041	4.71	NEG
18	M-H, M+FA-H	$C_{47}H_{76}O_{17}$	0.83	471.3469, 603.3911, 911.502	911.501	911.5017	9.03	NEG
19	M-H	$C_8H_8O_6S$	−0.07	74.0247, 151.0399, 172.0977, 230.9966	230.9969	230.9969	4.82	NEG
20	M-H	$C_{15}H_{14}O_7S$	−0.86	242.0586, 257.0821, 336.9946, 337.039	337.0387	337.0385	7.37	NEG
21	M-H	$C_{10}H_{12}O_5S$	0.24	57.0345, 79.9573, 131.0712, 163.0764, 174.9557, 243.0331	243.0333	243.0333	4.68	NEG
22	M+FA-H	$C_{19}H_{30}O8$	0.12	161.0454, 179.0562, 205.1229, 223.1336, 311.0563, 385.1873, 387.2024, 431.0975, 431.1887, 431.1961	431.1923	431.1923	4.48	NEG
23	M+H, M+K, M+Na	$C_{33}H_{40}O_{15}$	−0.81	71.0498, 85.029, 313.0708, 369.1337, 531.1862, 677.2408	677.244	677.2435	6.13	POS
24	M-H2O-H	$C_{17}H_{18}O_5$	4.03	222.9814, 239.1077, 242.9881, 262.9918, 268.0371, 282.9753, 282.9812, 283.0071, 283.0620, 283.0974	283.0977	283.0988	8.21	NEG
25	M-H, 2M-H	$C_{21}H_{20}O_{12}$	0.44	271.0248, 300.0275, 301.035, 463.0882	463.0882	463.0884	4.89	NEG
26	M-H	$C_{15}H_{18}O_3$	0.43		245.1183	245.1184	8.73	NEG
27	M-H	$C_{14}H_{20}O_9$	0.54		331.1035	331.1036	3.17	NEG
28	M-H	$C_{25}H_{30}O_8$	0.14		457.1868	457.1869	7.51	NEG
29	M-H	$C_{31}H_{36}O_{11}$	−1.06		583.2185	583.2179	9.01	NEG
30	M+Na	$C_{13}H_{18}O_7$	1.29		309.0944	309.0948	3.5	POS
31	M+FA-H	$C_{14}H_{16}O_2$	−0.15		261.1132	261.1132	9.07	NEG
32	M-H_2O-H	$C_8H_8O_7S$	0.12		228.9812	228.9813	4.71	NEG
33	M-H	$C_8H_8O_7S$	0.14		246.9918	246.9918	4.68	NEG
34	M-H_2O-H	$C_{11}H_{14}O_6$	0.24		223.0612	223.0613	5.1	NEG
35	M+FA-H	$C_{25}H_{26}O_{11}$	0.33		547.1457	547.1459	7.74	NEG
36	M+H	$C_{21}H_{20}O_6$	−0.88		369.1333	369.1329	9.09	POS
37	M-H	$C_{21}H_{20}O_6$	−0.09		367.1187	367.1187	7.61	NEG
38	M+H-H_2O, M+Na, M+H	$C_{21}H_{38}O_8$	−0.68		441.2459	441.2456	5.88	POS
39	M-H	$C_{15}H_{12}O_{11}S$	−0.45		399.0028	399.0026	4.65	NEG

40	M+FA-H	$C_{17}H_{16}O_5S$	0.16		377.07	377.0701	5.99	NEG
41	M-H	$C_{10}H_{12}O_6S$	−0.06		259.0282	259.0282	4.67	NEG
42	M+Na	$C_{26}H_{28}O_{12}$	−0.9		555.1473	555.1468	6.33	POS
43	M-H_2O-H	$C_{27}H_{32}O_{16}$	−0.72		593.1512	593.1508	4.68	NEG
44	M+Na	$C_{17}H_{24}O_{10}$	1.93		411.1261	411.1269	4.27	POS
45	M-H, M+FA-H	$C_{20}H_{23}NO_4$	0.57		340.1554	340.1556	4.55	NEG
46	M+FA-H	$C_{30}H_{44}O_{10}$	0.58		609.2916	609.292	10.59	NEG
47	M-H	$C_{27}H_{26}O_{19}$	1.91		653.0996	653.1008	4.59	NEG
48	M-H	$C_9H_6O_6S$	0.2		240.9812	240.9813	4.42	NEG
49	M-H	$C_{26}H_{34}O_{11}$	0.49		521.2028	521.2031	5.02	NEG
50	M+H	$C_{27}H_{28}O_{12}$	−0.76		545.1654	545.1649	8.44	POS
51	M-H	$C_{21}H_{18}O_{16}S$	−0.36		557.0243	557.0241	4.72	NEG
52	M+Na, M+K	$C_{14}H_{20}O_7$	−0.64		323.1101	323.1099	3.92	POS
53	M-H_2O-H	$C_{32}H_{30}O_{16}$	1.97		651.1356	651.1369	5.32	NEG
54	M+FA-H	$C_{33}H_{30}O_{16}$	−2.53		727.1517	727.1499	5.78	NEG
55	M+FA-H	$C_{16}H_{28}O_8$	1.34		393.1766	393.1771	4.78	NEG
56	M+FA-H	$C_{10}H_{16}O_2$	0.36		213.1132	213.1133	8.02	NEG
57	M+FA-H	$C_{18}H_{20}O_{10}$	−0.26		441.1039	441.1037	5.99	NEG
58	M-H_2O-H	$C_{17}H_{26}O_{11}$	0.81		387.1297	387.13	4.07	NEG
59	M+H-H_2O	$C_{31}H_{30}O_{16}$	1.15		641.1501	641.1509	4.67	POS
60	2M-H	$C_{16}H_{14}O_7$	1.77		635.1406	635.1418	5.21	NEG
61	M-H	$C_{28}H_{34}O_{14}$	0.44		593.1876	593.1878	5.12	NEG
62	M-H_2O-H	$C_{35}H_{32}O_{18}$	−3.01		721.141	721.1388	4.65	NEG
63	M-H_2O-H	$C_{15}H_{16}O_8S$	1.2		337.0388	337.0392	5.12	NEG
64	M+FA-H	$C_{25}H_{30}O_{11}$	0.56		551.177	551.1773	4.35	NEG
65	M-H	$C_{15}H_{22}O_5$	0.1		281.1394	281.1395	6.3	NEG
66	M-H_2O-H	$C_{15}H_{14}O_8S$	0.93		335.0231	335.0234	5.7	NEG
67	M+Na	$C_{26}H_{28}O_{13}$	−0.6		571.1422	571.1419	6.71	POS
68	M-H	$C_{26}H_{28}O_{13}$	0.46		547.1457	547.146	6.73	NEG
69	M+Na	$C_{27}H_{36}O_{15}S$	−0.09		655.1667	655.1667	4.65	POS
70	M+FA-H	$C_{19}H_{32}O_8$	1.42		433.2079	433.2085	4.52	NEG
71	M-H	$C_{19}H_{28}O_{11}$	0.38		431.1559	431.156	4.01	NEG
72	M-H_2O-H	$C_{26}H_{34}O_{13}$	0.41		535.1821	535.1823	4.87	NEG
73	M+FA-H	$C_{15}H_{12}O_{10}S$	−0.47		429.0133	429.0131	4.59	NEG
74	M+FA-H	$C_{23}H_{28}O_{11}$	0.58		525.1613	525.1616	4.68	NEG
75	M+FA-H	$C_{16}H_{24}O_7$	0.73		373.1504	373.1506	6.28	NEG
76	M-H	$C_{30}H_{46}O_7$	0.13		517.3171	517.3171	8.53	NEG
77	M-H	$C_{16}H_{26}O_8$	0.25		345.1555	345.1556	4.52	NEG
78	M+FA-H	$C_{19}H_{32}O_9$	0.35		449.2028	449.203	4.18	NEG
79	2M-H	$C_{17}H_{16}O_9$	−2.28		727.1516	727.1499	5.02	NEG
80	M-H	$C_{21}H_{22}O_9$	0.28		417.1191	417.1192	6.48	NEG
81	M+FA-H	$C_{14}H_{18}O_8$	0.42		359.0984	359.0985	3.74	NEG

(*Continued*)

https://doi.org/10.2147/DDDT.S530516

Table 1 (Continued).

No.	Adducts	Formula	Mass Error (ppm)	Fragment Ions	theoretical *m/z*	*m/z*	Rt /min	Ion mode
82	M-H_2O-H	$C_{15}H_{22}O_5$	0.37		263.1289	263.129	7.63	NEG
83	M+FA-H	$C_{13}H_{18}O_7$	0.86		331.1034	331.1037	3.77	NEG
84	M-H	$C_{16}H_{10}O_6$	4.38		297.0405	297.0418	6.67	NEG
85	M+FA-H	$C_6H_{12}O_2$	0.25		161.0819	161.082	4.22	NEG
86	M-H_2O-H	$C_{27}H_{42}O_5$	0.32		427.2854	427.2855	10.34	NEG
87	M-H_2O-H	$C_{27}H_{30}O_{14}S$	−3.38		591.1177	591.1157	5.14	NEG
88	M+Na	$C_{16}H_{24}O_7$	1.44		351.1414	351.1419	4.33	POS
89	M+FA-H	$C_{19}H_{34}O_9$	1.33		451.2184	451.219	4.26	NEG
90	M+FA-H	$C_{16}H_{30}O_8$	0.39		395.1923	395.1924	4.13	NEG
91	M-H	$C_{25}H_{30}O_9$	0.61		473.1817	473.182	6.42	NEG
92	M+FA-H	$C_{14}H_{20}O_2$	0.26		265.1445	265.1446	9.47	NEG
93	M+FA-H	$C_{32}H_{50}O_8$	0.83		607.3487	607.3492	9	NEG
94	M-H	$C_{12}H_{14}O_5$	0.35		237.0768	237.0769	6.54	NEG
95	M-H_2O-H	$C_{10}H_{14}O_5S$	0.62		227.0384	227.0385	6.33	NEG
96	M-H	$C_{10}H_{14}O_5S$	0.38		245.0489	245.049	4.57	NEG
97	M-H	$C_{11}H_{14}O_5$	0.53		225.0768	225.077	7.76	NEG
98	M+H, M+Na	$C_{39}H_{50}O_{19}$	−1.01		823.3019	823.3011	5.95	POS
99	M-H	$C_{27}H_{28}O_{12}$	−0.11		543.1508	543.1507	9.05	NEG
100	M+H	$C_{27}H_{28}O_{12}$	−0.63		545.1654	545.165	9.04	POS
101	M-H	$C_{11}H_{14}O_6S$	0.69		273.0438	273.044	5.91	NEG
102	M-H	$C_9H_{15}NO_3$	0.03		184.0979	184.0979	4.97	NEG
103	M+Na	$C_{21}H_{36}O_8$	−0.32		439.2302	439.2301	5.3	POS
104	M+Na	$C_{21}H_{38}O_8$	−0.24		441.2459	441.2458	5.35	POS
105	M-H	$C_{26}H_{34}O_{12}$	−0.13		537.1977	537.1977	5.02	NEG
106	M-H	$C_{15}H_{20}O_8$	0.37		327.1085	327.1087	4.05	NEG
107	M-H	$C_{15}H_{20}O_4$	−0.04		263.1289	263.1289	6.81	NEG
108	M-H	$C_{36}H_{26}O_{16}$	−4.32		713.1148	713.1117	5.38	NEG
109	M+H	$C_{10}H_{10}N_6O_6$	−0.03		311.0735	311.0734	2.39	POS
110	M-H	$C_{21}H_{30}O_8$	0.35		409.1868	409.1869	6.14	NEG
111	M+H-H_2O, M+H, M+Na	$C_{30}H_{48}O_5$	−0.16		511.3394	511.3393	9.51	POS
112	M-H	$C_{16}H_{24}O_{10}$	0.08		375.1297	375.1297	3.81	NEG
113	M-H_2O-H	$C_{19}H_{22}O_7S$	0.4		375.0908	375.0909	6.99	NEG
114	M-H_2O-H	$C_{20}H_{26}O_9$	0.95		391.1399	391.1402	5.12	NEG
115	M-H	$C_{10}H_7NO_4$	−0.17		204.0302	204.0302	3.86	NEG
116	M+H	$C_{20}H_{20}O_6$	−0.42		357.1333	357.1331	7.6	POS
117	M-H	$C_{20}H_{24}O_6$	−0.12		359.15	359.15	8.83	NEG
118	M+Na, M+K	$C_{16}H_{28}O_7$	0.17		355.1727	355.1728	4.77	POS
119	M+FA-H	$C_{21}H_{26}O_4$	0.64		387.1813	387.1815	9.74	NEG
120	M-H	$C_{27}H_{32}O_{12}$	0.01		547.1821	547.1821	5.87	NEG
121	M-H_2O-H	$C_{32}H_{48}O_7$	−3.82		525.3221	525.3201	9.59	NEG
122	M-H	$C_{25}H_{28}O_8$	0.03		455.1711	455.1712	8.14	NEG

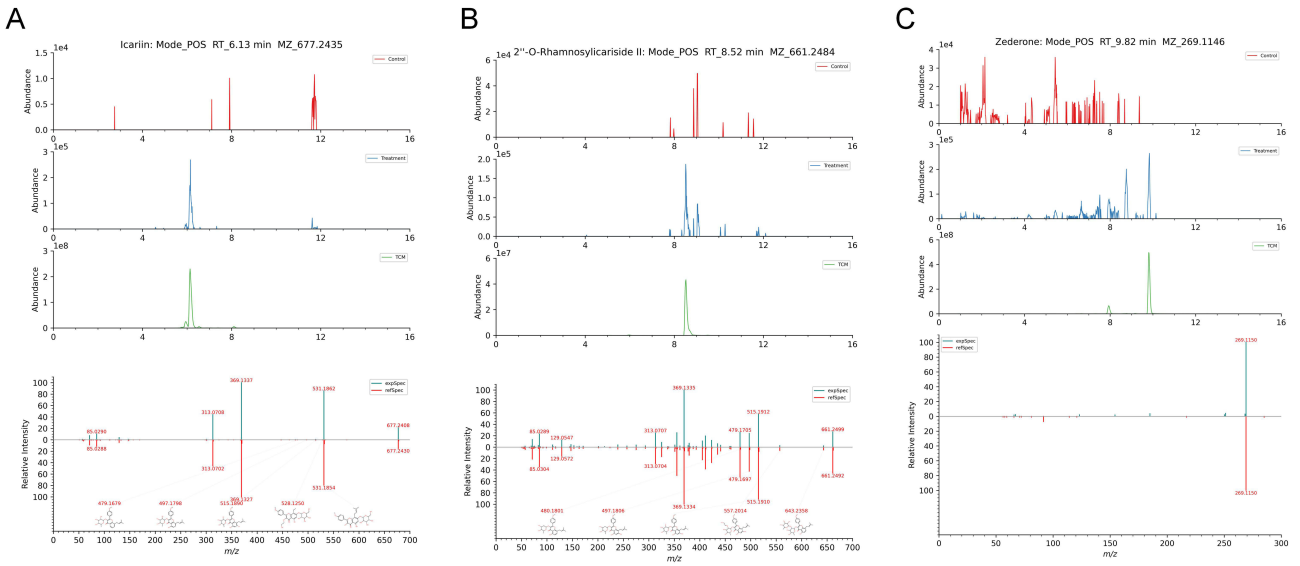

Figure 5 EIC and MS/MS spectrum compared with databases in mice serum. (**A**) Icariin. (**B**) 2''-O-Rhamnosylicariside. (**C**) Zederone.

involving 2''-O-Rhamnosylicariside II, epimedin C can be bioconverted into Icariin, providing an efficient and straightforward approach for the industrial production of Icariin.[19]

Zederone

The detection of Zederone in serum revealed a significant ion peak at *m/z* 269.1146 with a retention time of 9.82 minutes, where the peak intensity in the TCM group was markedly higher than that in the control and treated groups. A highly consistent fragment ion peak was observed in the control spectrum, with *m/z* 269.1150 providing a distinct characteristic for this component. The scores and fragmentation scores for Zederone were 69.4 and 87.7, respectively, and a mass error of −0.83 ppm further demonstrated the accuracy and reliability of the analysis. Studies have shown that Zederone can suppress the growth of SKOV3 via the mTOR/p70s6K pathway.[20] It has been reported that Zederone can improve the fecal microbial distribution in dementia model rats, regulate the biological dysfunction of intestinal flora, and might be a strong contender for the treatment of dementia and similar neurological illnesses.[21] In toxicity experiments investigating Zederone, it was found that 223 mg/kg was the lethal dose of Zederone after injecting adult male mice with it for 24 hours.[22] Meanwhile, zederone exhibited notable anti-inflammatory activity.[23]

Identification of Metabolites

Drug metabolism, also known as biotransformation of drugs, primarily occurs in the liver and involves orderly chemical changes to drugs. This process is divided into Phase I and Phase II metabolism. Phase I metabolism increases the polarity of compounds or exposes polar groups through reactions such as oxidation, reduction and hydrolysis, enabling some compound to be directly excreted. However, most compounds require further Phase II metabolism, which involves conjugation with endogenous substances in the body, such as glucuronic acid, sulfuric acid, amino acids, or undergoing acetylation and methylation reactions, to facilitate excretion or reduce toxicity, ensuring orderly body functions. Different structural types of compounds undergo different metabolic reactions in the body. By comparing the exact molecular weights from primary mass spectrometry, secondary mass spectrometry fragments, isotope distributions, and retention times, using positive ion detection mode, 62 metabolites were identified in the serum of biological samples from the drug-administered group. Specific information is provided in Table 2. Table 2 presents the retention time, matching score and so on. Generally, prototype components can be directly eliminated via phase I metabolism or further excreted via phase II metabolic reactions.[24,25] The characterized constituents exhibited an error margin of less than 5 ppm, with only a few prototype components being absorbed.

https://doi.org/10.2147/DDDT.S530516

Table 2 Identification of Serum Metabolites

No.	Mid	Retention Time (min)	Fragmentation Score	Mass Error (ppm)	Formula	Metabolites
86	M1	10.34	0	0.32	$C_{27}H_{42}O_5$	(25S)-12beta-Hydroxyspirost-4-en-3-one_M1
87	M1	5.14	0.0245	−3.38	$C_{27}H_{30}O_{14}S$	(2S)-Isoxanthohumol_M1
91	M1	6.42	0	0.61	$C_{25}H_{30}O_9$	(5R,6E)-5-Hydroxy-1,7-diphenyl-6-hepten-3-one_M1
1	M1	5.01	69.9	−1.15	$C_{32}H_{34}O_{18}$	1,4-Dicaffeoylquinic acid_M1
93	M1	9.00	0.00403	0.83	$C_{32}H_{50}O_8$	23(R)-16beta-hydroperoxyalisol B 23-acetate_M1
113	M1	6.99	0	0.40	$C_{19}H_{22}O_7S$	4-O-Methyl honokiol_M1
116	M1	7.60	0	−0.42	$C_{20}H_{20}O_6$	6-Prenylapigenin_M1
117	M1	8.83	0	−0.12	$C_{20}H_{24}O_6$	7-Geranyloxy-5-methoxycoumarin_M1
5	M1	4.05	51	0.92	$C_{10}H_{12}O_7S$	Acetosyringone_M1
119	M1	9.74	3.21	0.64	$C_{21}H_{26}O_4$	Acitretin_M1
121	M1	9.59	0	−3.82	$C_{32}H_{48}O_7$	Alisol C 23-acetic acid_M1
122	M1	8.14	0	0.03	$C_{25}H_{28}O_8$	Alnustone_M1
120	M1	5.87	0	0.01	$C_{27}H_{32}O_{12}$	Arctigenin_M1
97	M1	7.76	0	0.53	$C_{11}H_{14}O_5$	Bancroftinone_M1
101	M1	5.91	41.5	0.69	$C_{11}H_{14}O_6S$	Beta-asarone_M1
96	M1	4.57	44.5	0.38	$C_{10}H_{14}O_5S$	Carvacrol_M1
8	M1	5.47	71.1	3.99	$C_{24}H_{28}O_{12}$	Colutehydroquinone_M1
108	M1	5.38	0	−4.32	$C_{36}H_{26}O_{16}$	Cupressuflavone_M1
110	M1	6.14	0	0.35	$C_{21}H_{30}O_8$	Cyperenone_M1
95	M1	6.33	47.4	0.62	$C_{10}H_{14}O_5S$	D(+)-Carvone_M1
84	M1	6.67	0	4.38	$C_{16}H_{10}O_6$	Damnacanthol_M1
10	M1	4.24	76.8	0.57	$C_9H_6O_7S$	Daphnetin_M1
37	M1	7.61	0	−0.09	$C_{21}H_{20}O_6$	Dehydroglyasperin C_M1
39	M1	4.65	20.7	−0.45	$C_{15}H_{12}O_{11}S$	Dihydromyricetin_M1
40	M1	5.99	0.0035	0.16	$C_{17}H_{16}O_5S$	Effusol_M1
41	M1	4.67	41	−0.06	$C_{10}H_{12}O_6S$	Eugenol acetate_M1
42	M1	6.33	0	−0.90	$C_{26}H_{28}O_{12}$	Fargesin_M1
46	M1	10.59	0	0.58	$C_{30}H_{44}O_{10}$	Ginkgolic Acid 17:2_M1
47	M1	4.59	0	1.91	$C_{27}H_{26}O_{19}$	Herbacetin_M1
48	M1	4.42	0	0.20	$C_9H_6O_6S$	Herniarin_M1
14	M1-1	8.45	77.5	0.51	$C_{27}H_{28}O_{12}$	Icaritin_M1-1
50	M1-2	8.44	26.5	−0.76	$C_{27}H_{28}O_{12}$	Icaritin_M1-2
26	M1	8.73	0	0.43	$C_{15}H_{18}O_3$	Kauniolide_M1
29	M1	9.01	0	−1.06	$C_{31}H_{36}O_{11}$	Kushenol A_M1
28	M2	7.51	0	0.14	$C_{25}H_{30}O_8$	Kushenol A_M2
16	M1	6.46	93.1	−0.91	$C_{26}H_{26}O_{12}$	Licoisoflavone A_M1
17	M1	4.71	88	−0.81	$C_{27}H_{26}O_{18}$	Luteolin_M1
19	M1	4.82	72.9	−0.07	$C_8H_8O_6S$	Methyl Paraben_M1
32	M2	4.71	0	0.12	$C_8H_8O_7S$	Methyl Paraben_M2
33	M1	4.68	0	0.14	$C_8H_8O_7S$	Methyl protocatechuate_M1
35	M1	7.74	0.0211	0.33	$C_{25}H_{26}O_{11}$	Methylophiopogonone B_M1
51	M1	4.72	0	−0.36	$C_{21}H_{18}O_{16}S$	Morin_M1
67	M1-1	6.71	0	−0.60	$C_{26}H_{28}O_{13}$	Noricaritin_M1-1
68	M1-2	6.73	1.55	0.46	$C_{26}H_{28}O_{13}$	Noricaritin_M1-2
69	M1	4.65	0	−0.09	$C_{27}H_{36}O_{15}S$	Octahydrocurcumin_M1
20	M1	7.37	77.8	−0.86	$C_{15}H_{14}O_7S$	Ononetin_M1
73	M1	4.59	0	−0.47	$C_{15}H_{12}O_{10}S$	Padmatin_M1
75	M1	6.28	0	0.73	$C_{16}H_{24}O_7$	Perillyl alcohol_M1
66	M1	5.70	0	0.93	$C_{15}H_{14}O_8S$	Phloretin_M1
79	M1	5.02	0.217	−2.28	$C_{17}H_{16}O_9$	Plumbagin_M1

(*Continued*)

Table 2 (Continued).

No.	Mid	Retention Time (min)	Fragmentation Score	Mass Error (ppm)	Formula	Metabolites
80	M1	6.48	0	0.28	$C_{21}H_{22}O_9$	Pteryxin_M1
21	M1	4.68	52	0.24	$C_{10}H_{12}O_5S$	Raspberry ketone_M1
53	M1	5.32	0	1.97	$C_{32}H_{30}O_{16}$	Salvianolic acid A_M1
54	M1	5.78	0	−2.53	$C_{33}H_{30}O_{16}$	Salvianolic acid C_M1
57	M1	5.99	10.3	−0.26	$C_{18}H_{20}O_{10}$	Senkyunolide C_M1
59	M1	4.67	0	1.15	$C_{31}H_{30}O_{16}$	Silychristin_M1
60	M1	5.21	0	1.77	$C_{16}H_{14}O_7$	Steppogenin_M1
61	M1	5.12	11.8	0.44	$C_{28}H_{34}O_{14}$	Syringaresinol_M1
62	M1	4.65	0	−3.01	$C_{35}H_{32}O_{18}$	Theaflavin_M1
63	M1	5.12	0	1.20	$C_{15}H_{16}O_8S$	Toddaculin_M1
99	M1-1	9.05	0	−0.11	$C_{27}H_{28}O_{12}$	beta-Anhydroicaritin_M1-1
100	M1-2	9.04	0	−0.63	$C_{27}H_{28}O_{12}$	beta-Anhydroicaritin_M1-2

Table 3 The Lowest Free Energy of the Top 5 Models for the Docking of Icariin with the Core Target Molecule

Target Name	Docking Energy / kcal·mol^{-1}				
CA12	−7.5	−7.5	−7.1	−7.1	−7
ADORA1	−9	−8.7	−8.5	−7.8	−7.7
AKR1B1	−8.3	−8.2	−8	−7.7	−7.7
CA2	−7.3	−7.1	−6.9	−6.7	−6.7
ADORA2	−7.6	−7.2	−7.2	−7.2	−6.9
ADORA3	−8.1	−7.7	−7.6	−7.3	−7.3

Metabolic reactions are generally categorized into Phase I and Phase II. Previous reactions modify the molecular structure of drugs or exogenous components, increasing their polarity and thereby facilitating their excretion from the body. For example, ginsenosides, as a typical active component of TCM, must undergo Phase I metabolic transformations such as deglycosylation and dehydration to penetrate the intestinal mucosa and enter the bloodstream, thereby exerting their pharmacological effects.[26,27] Experimental findings demonstrated that ginsenoside Rh2 significantly delayed BC growth and metastasis by enhancing the cytotoxicity of NK cells.[28] Furthermore, the biotransformation of geniposide in the body involves both Phase I and Phase II reactions, with the Phase I reaction phase mainly consisting of hydrolysis reactions. Genipin can be its primary hydrolysis product,[29,30] and it has been shown to inhibit the growth of BC.[31] In contrast to Phase I metabolism, Phase II metabolic reactions primarily include conjugation reactions such as methylation, sulfation, and glucuronidation, which further increase the polarity of molecules, making them more readily excretable The metabolic reactions in serum follow a similar pattern, with some components sequentially undergoing both phases: first, molecular structure modification and increased polarity through Phase I reactions (eg, oxidation, reduction, hydrolysis), followed by Phase II reactions (eg, methylation, sulfation, glucuronidation) for further modification, ultimately forming highly polar metabolites. This synergistic metabolic mechanism not only expands the pathways of biotransformation but also significantly enhances the water solubility of metabolites, thereby promoting their efficient excretion from the body.[24]

Metabolic reactions in serum are dynamic and complex. Different components may undergo distinct metabolic pathways, and even the same component may exhibit varying metabolic characteristics at different time points. For instance, some components may only undergo Phase I reactions, while others may experience both Phase I and Phase II reactions. This diversity reflects the intricate metabolic network of TCM components within the body and provides critical insights into the dynamic changes of metabolites in serum. Through in-depth research on these metabolic

pathways, we can gain a better understanding of the pharmacodynamic material basis and mechanisms of action of TCM components.

For instance, β-asarone, a key metabolite identified in serum, has derivatives that inhibit BC cells.[32] β-asarone was identified at *m/z* 273.0440 in negative ion mode at 5.91 minutes, and its possible molecular formula is inferred to be $C_{11}H_{14}O_6S$ (with a Mass Error of 0.69). The metabolic process primarily involves demethylation, a Phase I metabolic reaction (Figure 6). By removing methyl groups, the chemical structure and biological activity of the drug molecule are altered, and sometimes this change may increase or decrease the pharmacological effect of the drug.[33] Subsequently, as a Phase II metabolic reaction, sulfation adds a sulfate group to the drug molecule, which not only further increases the polarity of the molecule and enhances its water solubility but also typically leads to the inactivation of the drug, making it more readily metabolized and excreted from the body. This process helps to regulate the concentration of the drug in the body, and reduce the toxic. Besides, it ensure that the active components of the drug can exert their intended therapeutic

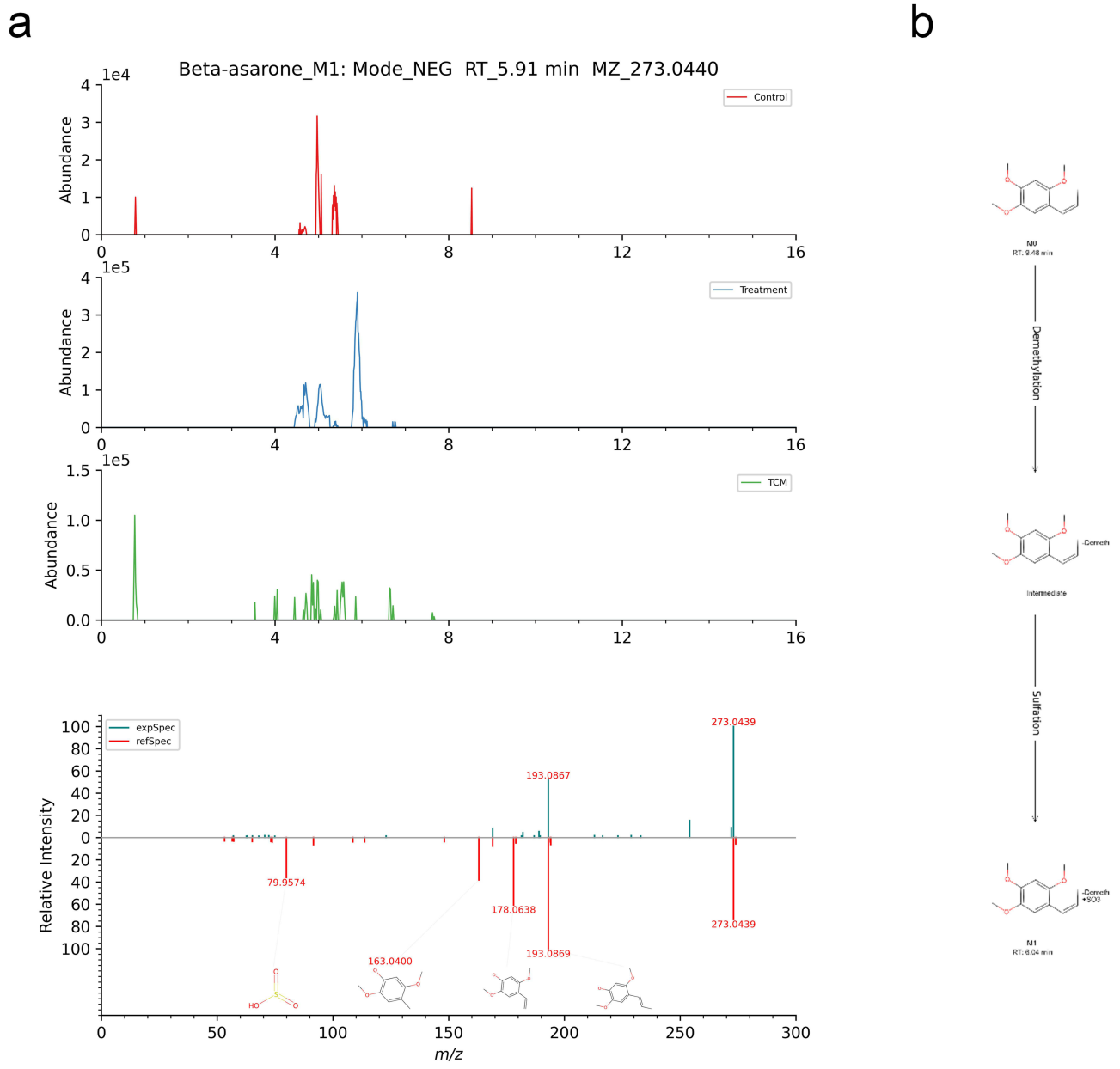

Figure 6 Identification of metabolite number 101. (**a**) EICs of metabolites and MS/MS spectra of reference compounds. (**b**) Network diagram for metabolites.

effects.[34] The component classification and quantitative distribution of metabolic components of XLCF in mouse serum are presented in Figure 7.

2.4 Screening of the targets and potential mechanism of XLCF to BC based on network pharmacology and molecular docking

We retrieved component information, including SMILES and InChiKeys, from the HERB database. Then, we predicted the pharmacological properties of these components via the SwissADME website and filtered out 43 bioactive components. Subsequently, we predicted potential targets for these bioactive components using the SwissTargetPrediction website, with the top 20 targets designated as potential action targets (Supplementary Table 2).We retrieved disease-related targets by searching "breast cancer" on the GeneCards website (Supplementary Table 3). As shown in the Venn diagram in Figure 8, 400

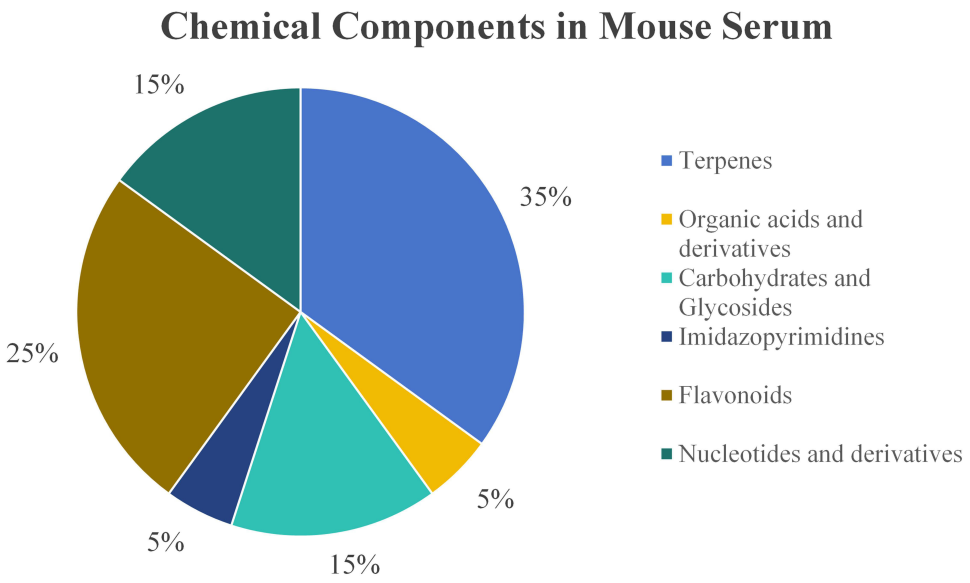

Figure 7 Statistics of Traditional Chinese Medicine Components Classifiable in serum of mice.

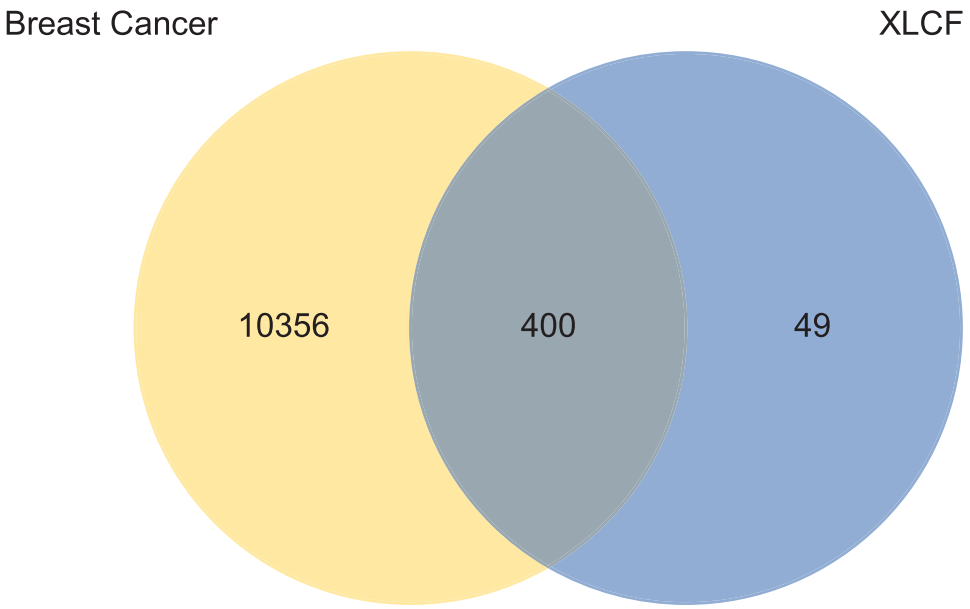

Figure 8 Venn diagram of breast cancer targets and XLCF target.

https://doi.org/10.2147/DDDT.S530516

overlapping targets were identified between the disease and drug targets (Supplementary Table 4). GO and KEGG analyses suggested that XLCF may exert its effects by regulating signal transduction pathways (such as PI3K-Akt, MAPK, etc)., inflammatory and immune-related pathways (such as AGE-RAGE, T-cell receptors), and cellular metabolic-related pathways (such as Protein phosphorylation). Please refer to Figures 9 and 10 for more details. On the STRING database, we analyzed the overlapping target proteins and selected the top 25 proteins with the highest degrees of connectivity (Figure 11). The core proteins included GAPDH, AKT1, TP53, ALB, TNF, and MAPK3. We visualized the relationships among drugs, active

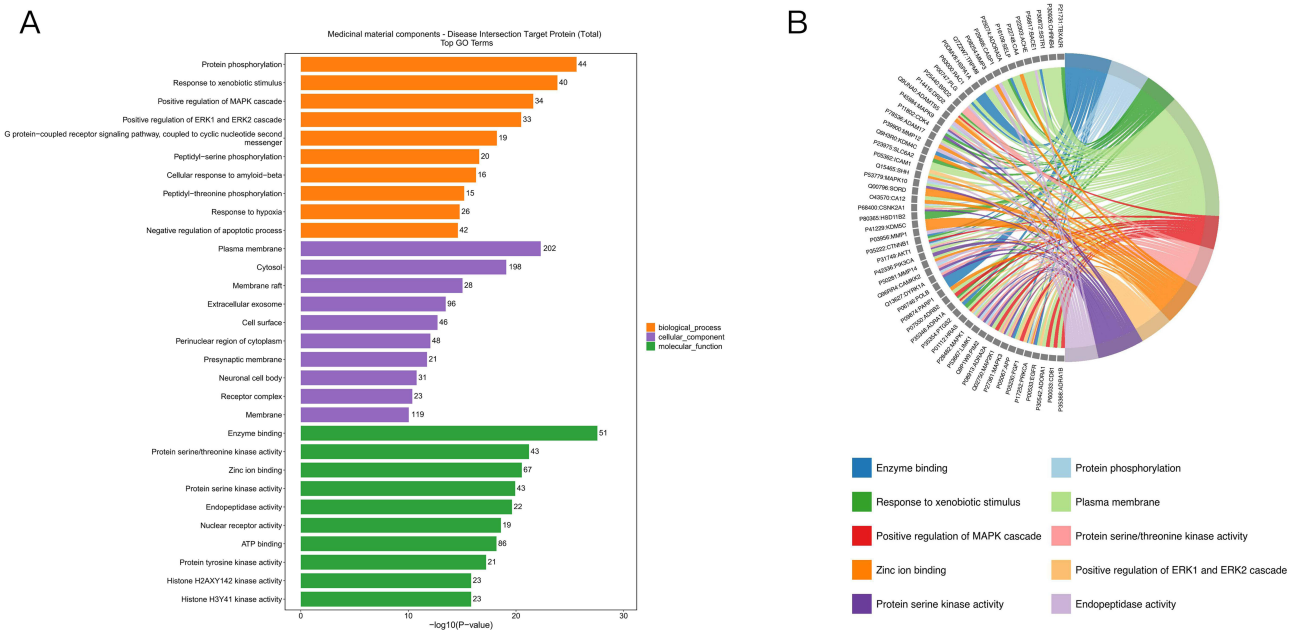

Figure 9 Enrichment analysis of GO of 400 common targets of XLCF and breast cancer. (**A**) Top30 bar chart for GO enrichment analysis. (**B**) GO enrichment analysis chord graph.

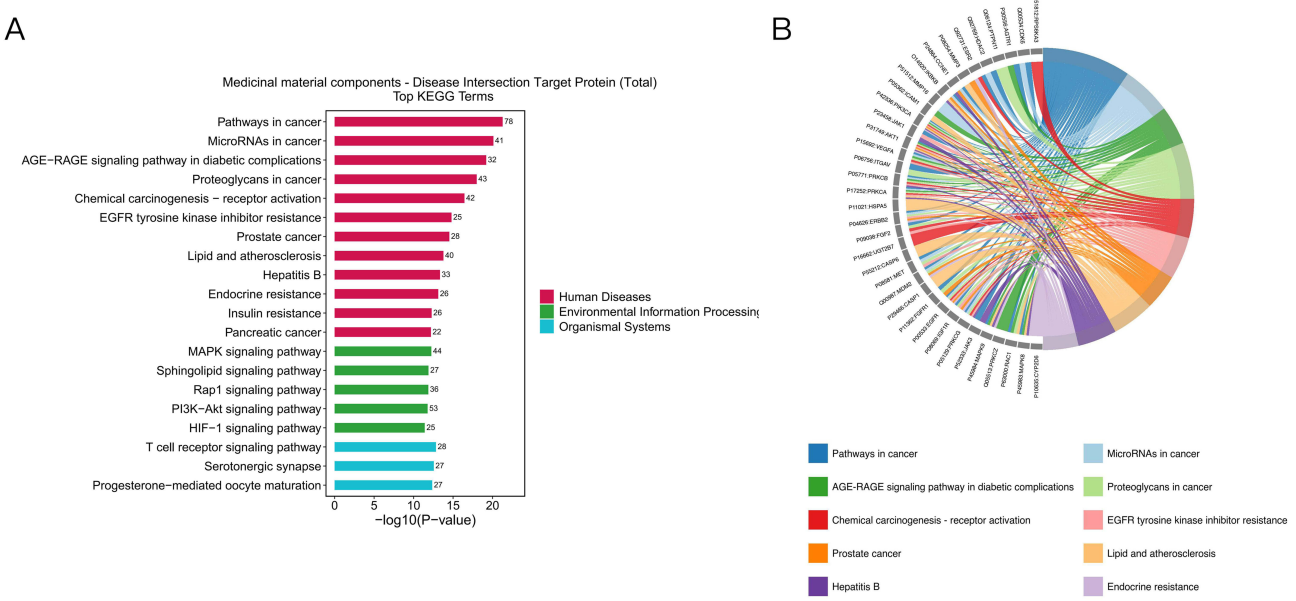

Figure 10 Enrichment analysis of KEGG of 400 common targets of XLCF and breast cancer. (**A**) KEGG enrichment analysis top20 bar chart. (**B**) KEGG enrichment analysis chord graph.

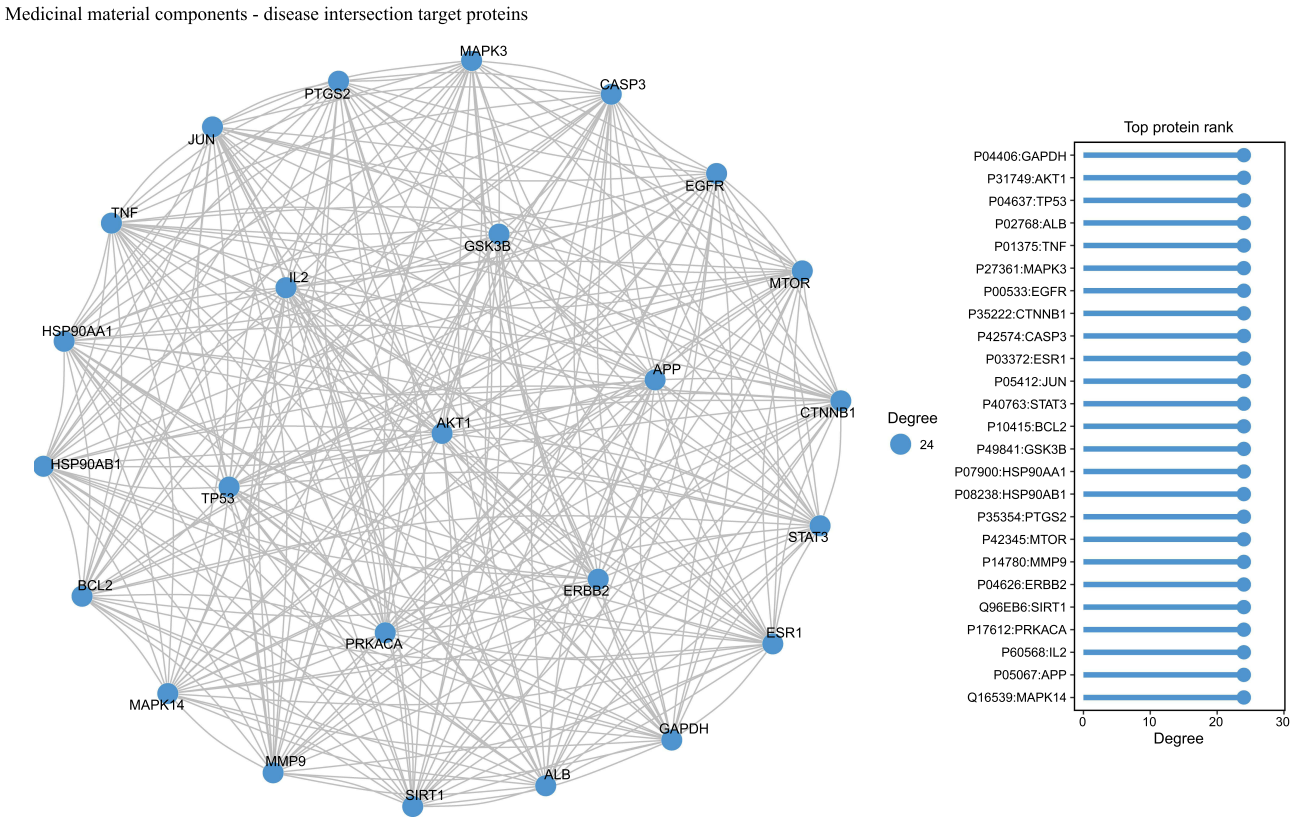

Figure 11 PPI network diagram.

components, targets, and diseases to construct a PPI network, which helped assess the relevance and importance of XLCF's active components to their targets (Figure 12). The top five core targets were CA12, ADORA1, AKR1B1, CA2, and ADORA2 and ADORA3. The core active components were isoquercetrin, Herbacetin_M1, beta-Anhydroicaritin_M1-1, Icaritin_M1-1, beta-Anhydroicaritin_M1-2, Baohuoside VI, and Icariin. We also used the top 25 KEGG enrichment pathways to create a Sankey diagram, which illustrated the associations between XLCF components and their corresponding targets in various pathways (Figure 13). Based on the aforementioned study, we selected Icariin and for molecular docking with the core targets (CA12, ADORA1, AKR1B1, CA2, ADORA2, ADORA3). The results indicated that the binding free energy of Icariin with these core targets was all less than −5.0 kcal/mol, suggesting good binding activity. Details are shown in Table 3. Among them, the docking effect of Icariin with ADORA1, AKR1B1 and ADORA3 were the best (Figure 14).This is consistent with the statements in the literature.[35–37]

Discussion

Among women, BC is a highly prevalent cancer. In 2019, BC accounted for 15.2% of new cancer cases and 6.9% of cancer-related deaths per 100,000 cases. Notably, over 90% of these deaths were caused by recurrence and metastasis.[7,8,38] Common metastatic sites include the lungs, bones, liver, and brain.[9,39] Therefore, investigating the pathological mechanisms of BC metastasis and developing effective therapeutic drugs are of significant practical importance.

Based on previous research conducted by our team, the concept of "phlegm-toxin-stasis" as an etiological factor and pathological product has been found to play a critical role throughout the development and progression of BC. Consequently, the therapeutic approach of "resolving stasis and detoxifying", which targets the primary pathogenesis of phlegm-toxin-stasis, has been widely applied in postoperative anti-recurrence and anti-metastasis treatment of BC, demonstrating certain clinical efficacy. Through extensive clinical trials, XLCF has shown definitive therapeutic effects against BC. It has been used for over a decade at Longhua Hospital affiliated with Shanghai University of TCM with favorable outcomes. Experimental studies have indicated that XLCF can alleviate BC metastasis by inhibiting M2

https://doi.org/10.2147/DDDT.S530516

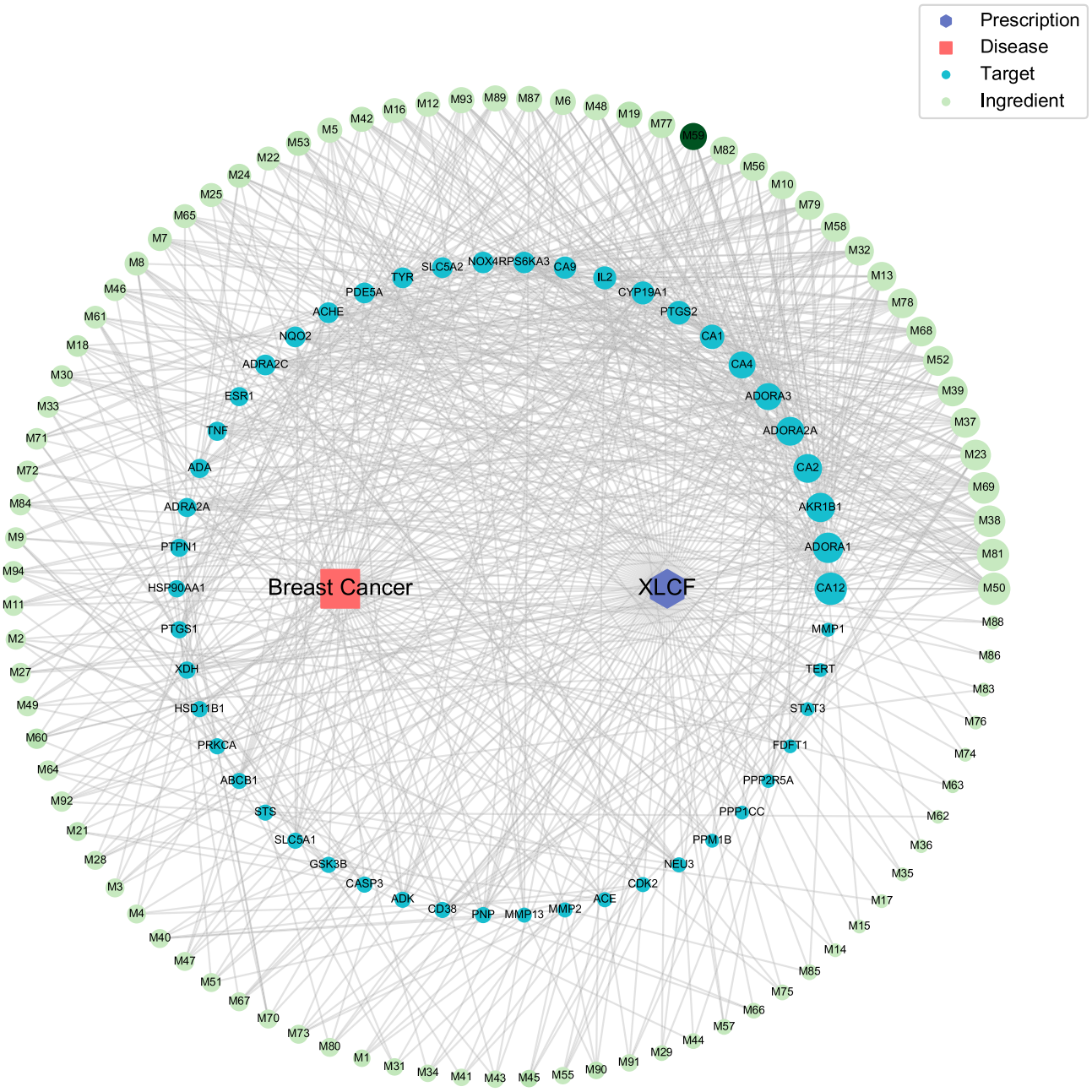

Figure 12 Medicinal materials - Components - Targets - disease map.

macrophage polarization. Furthermore, MTT, Scratch assays, and Transwell assays have revealed that XLCF effectively suppresses the proliferation, migration, and invasion capabilities of BC cells.[40]

In this study, we employed UHPLC-Q-Exactive Orbitrap-MS to comprehensively profile the metabolome of XLCF, definitively characterizing 913 chemical components and identifying 122 blood-absorbable prototypes, including terpenes, flavonoids, carbohydrates, nucleotides, and organic acids. Terpenes (35%) and flavonoids (25%) were the predominant classes, suggesting their role as primary bioactive constituents. This metabolomic analysis not only delineates chemical composition of XLCF but also provides a foundation for investigating its anti-BC mechanisms.

The identified bioactive components and their associated metabolic pathways collectively elucidate the pharmacological basis of XLCF's therapeutic effects. For instance, literature research has confirmed that Flavonoid compounds can exert anti-tumor effects by inducing apoptosis, scavenging reactive oxygen species, and altering metabolic pathways.[41,42]

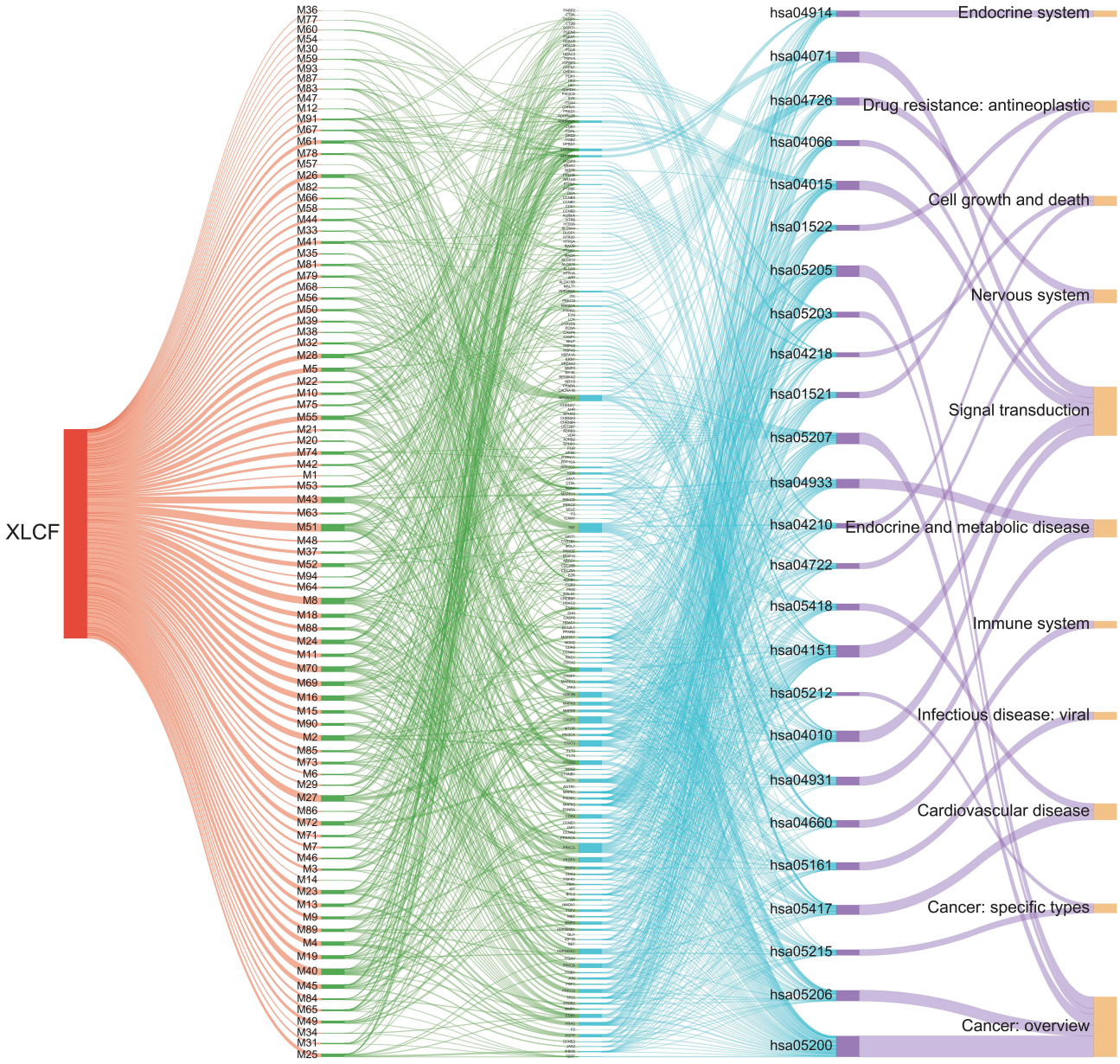

Figure 13 Sankey Graph.

Terpenoid compounds have also been proven to effectively combat cancer.[43] This provides a good means to investigate the mechanism underlying XLCF in combating the metastasis of BC. Research has confirmed that Icariin can inhibit TNBC through the SIRT6/NF-κB signaling pathway.[18] Meanwhile, We have proposed that asiaticoside can exert an anti-BC effect by inhibiting the inflammatory pathway.[12,13] Baohuoside V can also inhibit the proliferation of BC cells in a dose-induced manner.[14] The identification of these bioactive components and their metabolic pathways through metabolomic profiling highlights the potential of XLCF in modulating the tumor microenvironment and enhancing immune responses against BC.

Moreover, the metabolomic analysis revealed 62 metabolic products in the serum of mice include glucuronidation, hydroxylation, sulfation, demethylation, methylation, oxidation, deacetylation, epoxide_hydrolysis, Isopropenyl_oxidation and vinyl_oxidation. Among these, the main metabolic reactions include glucuronidation, hydroxylation, and sulfation. These findings are significant as they demonstrate how the components of XLCF are metabolized

https://doi.org/10.2147/DDDT.S530516

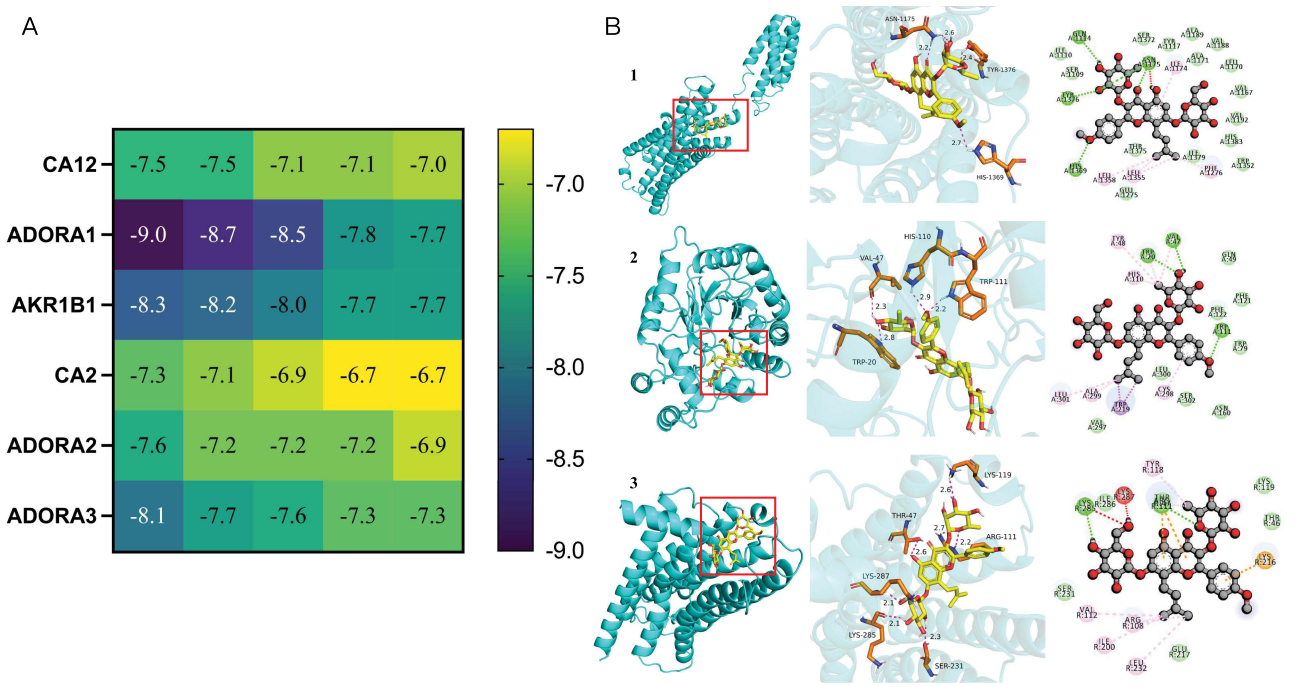

Figure 14 Molecular docking results. (**A**) The heat map of molecule docking scores. (**B**) Molecular models of Icariin binding to the predicted targets. 1. ADORA1; 2. AKR1B1; 3. ADORA3.

in the body and how these metabolites may contribute to the overall therapeutic effects of XLCF. For example, although glucuronidation was once considered a biological waste excreted through urine in earlier times, many recent studies have found that it can play a role in improving the effects on breast tumors in the field of antibody-drug conjugates and nanomedicine, meanwhile, reducing the toxic effects of Western medicines.[44] Literature has discovered the existence of histone hydroxylation modification (H3P16oh) in mammals, and identified EGLN2 as the histone hydroxylase responsible for this modification. Subsequent research by the authors on the function of histone hydroxylation in TNBC revealed that the EGLN2-H3P16oh-KDM5A pathway can activate WNT/β-catenin signaling in TNBC by regulating the negative regulator of the WNT/β-catenin pathway.[45] It has been reported that arylsulfatase D (ARSD), as a new downstream target gene of ERα, can curb the expansion and motility of BC cells via activating the Hippo/YAP signaling pathway.[46] Therefore, metabolic product analysis is beneficial for revealing the high reactivity of metabolic products, and it also reflects how TCM components can increase their bioavailability and activity by adding polar groups. This further underscores the importance of understanding the metabolic pathways of TCM components, as they can provide valuable information for optimizing therapeutic strategies.

We further explored the inhibitory effect of XLCF on BC by using network pharmacology and molecular docking, and found that it might be related to inflammation, cell metabolism, etc. Icariin, a terpene compound, was selected to dock with the core target molecule. Computational analysis identified robust molecular interactions with ADORA1, AKR1B1 and ADORA3, suggesting these targets mediate the compound's pharmacological effects. This study further confirmed the potential role of XLCF in inhibiting BC.

This study combined UHPLC-MS metabolomics and network pharmacology to systematically analyze the anti-BC mechanism of XLCF, and identified 122 active components entering the blood. Among them, Icaritin (a metabolite of *Epimedium brevicornu Maxim*) due to its high bioavailability and strong binding ability to BC targets (ADORA1, AKR1B1, ADORA3), Become a key active molecule. Bioinformatic pathway analysis revealed that XLCF likely exerts anti-BC activity by coordinately regulating inflammatory response pathways and metabolic reprogramming processes, in agreement with previously reported TNBC suppression by Icaritin. Although the results of this paper provide a potential

pharmacological basis, in the future, it is still necessary to further clarify the specific targets and molecular mechanisms of the anti-breast tumor effect of XLCF based on this work by using proteomics technology and PROTAC probes.

Data Sharing Statement

Data are contained within the article and Supplementary Tables 1–4.

Author Contributions

All authors made a significant contribution to the work reported, whether that is in the conception, study design, execution, acquisition of data, analysis and interpretation, or in all these areas; took part in drafting, revising or critically reviewing the article; gave final approval of the version to be published; have agreed on the journal to which the article has been submitted; and agree to be accountable for all aspects of the work.

Funding

This work was supported by National Natural Science Foundation of China (No. 82205132, 82474508).

Disclosure

The authors declare no conflicts of interest.

References

1. Nolan E, Kang Y, Malanchi I. Mechanisms of organ-specific metastasis of breast cancer. *Cold Spring Harb Perspect Med*. 2023;13(11):a041326. doi:10.1101/cshperspect.a041326
2. US Preventive Services Task Force, Nicholson WK, Silverstein M, Wong JB, et al. Screening for breast cancer: US Preventive Services Task Force recommendation statement. *JAMA*. 2024;331(22):1918–1930. doi:10.1001/jama.2024.5534
3. von Minckwitz G, Huang CS, Mano MS, et al. Trastuzumab emtansine for residual invasive HER2-positive breast cancer. *N Engl J Med*. 2019;380(7):617–628. doi:10.1056/NEJMoa1814017
4. Liu Y, Xu J, Ge C, et al. Physicochemical properties, structural analysis, and activity of Shancigu polysaccharides. *Int J Biol Macromol*. 2025;298:140071. doi:10.1016/j.ijbiomac.2025.140071
5. Ye Y, Pei L, Wu C, et al. Protective effect of Traditional Chinese Medicine formula RP on lung microenvironment in pre-metastasis stage of breast cancer. *Integr Cancer Ther*. 2019;18:1534735419876341. doi:10.1177/1534735419876341
6. Xie RF, Liu S, Yang M, et al. Effects and possible mechanism of Ruyiping formula application to breast cancer based on network prediction. *Sci Rep*. 2019;9(1):5249. doi:10.1038/s41598-019-41243-9
7. Evans-Knowell A, LaRue AC, Findlay VJ. MicroRNAs and their impact on breast cancer, the tumor microenvironment, and disparities. *Adv Cancer Res*. 2017;133:51–76.
8. Chaffer CL, Weinberg RA. A perspective on cancer cell metastasis. *Science*. 2011;331(6024):1559–1564. doi:10.1126/science.1203543
9. Xiao M, Yang S, Meng F, et al. LAPTM4B predicts axillary lymph node metastasis in breast cancer and promotes breast cancer cell aggressiveness in vitro. *Cell Physiol Biochem*. 2017;41(3):1072–1082. doi:10.1159/000464115
10. Li X, Wang P, Tong Y, et al. UHPLC-Q-Exactive Orbitrap MS/MS-based untargeted metabolomics and molecular networking reveal the differential chemical constituents of the bulbs and flowers of Fritillaria thunbergii. *Molecules*. 2022;27(20):6944. doi:10.3390/molecules27206944
11. Wang H, Wu Y, Xiang H, et al. UHPLC-Q-Exactive Orbitrap MS/MS-based untargeted lipidomics reveals molecular mechanisms and metabolic pathways of lipid changes during golden pomfret (Trachinotus ovatus) fermentation. *Food Chem*. 2022;396:133676. doi:10.1016/j.foodchem.2022.133676
12. Guo M, Ying Y, Chen Y, et al. Asiaticoside inhibits breast cancer progression and tumor angiogenesis via YAP1/VEGFA signal pathway. *Heliyon*. 2024;10(18):e37169. doi:10.1016/j.heliyon.2024.e37169
13. Al-Saeedi FJ. Asiaticoside increases Caspase-9 Activity in MCF-7 cells and inhibits TNF-α and IL-6 expression in nude mouse xenografts via the NF-κB pathway. *Molecules*. 2023;28(5):2101. doi:10.3390/molecules28052101
14. Wang T, Zhang JC, Chen Y, et al. [Comparison of antioxidative and antitumor activities of six flavonoids from Epimedium koreanum]. *Zhongguo Zhong Yao Za Zhi*. 2007;32(8):715–718.
15. Petrova M, Dimitrova L, Dimitrova M, et al. Antitumor and antioxidant activities of in vitro cultivated and wild-growing Clinopodium vulgare L. *Plants*. 2023;12(8):1591. doi:10.3390/plants12081591
16. Stary D, Bajda M. Taurine and creatine transporters as potential drug targets in cancer therapy. *Int J Mol Sci*. 2023;24(4):3788. doi:10.3390/ijms24043788
17. De-Simone SG, de Salles CM, Batista e Silva CM, et al. Purification and amino acid sequence of fructose-1,6-bisphosphate aldolase from the electric organ of Electrophorus electricus (L.). *Z Naturforsch C J Biosci*. 2006;61(11–12):884–888. doi:10.1515/znc-2006-11-1217
18. Song L, Chen X, Mi L, et al. Icariin-induced inhibition of SIRT6/NF-κB triggers redox mediated apoptosis and enhances anti-tumor immunity in triple-negative breast cancer. *Cancer Sci*. 2020;111(11):4242–4256. doi:10.1111/cas.14648
19. Lyu Y, Zeng W, Du G, et al. Efficient bioconversion of epimedin C to icariin by a glycosidase from Aspergillus nidulans. *Bioresour Technol*. 2019;289:121612. doi:10.1016/j.biortech.2019.121612
20. Zhang Z, Li L, Wang J, et al. A study of zederone for the inhibition on ovarian cancer cell proliferation through mTOR/p70s6K signalling pathway. *J BUON*. 2020;25(2):785–791.

21. Borah S, Sarkar P, Sharma HK. Zederone improves the fecal microbial profile in dementia induced rat model: a first report. *CNS Neurol Disord Drug Targets*. 2022;21(4):335–342. doi:10.2174/1871527320666210827114227
22. Pimkaew P, Suksen K, Somkid K, et al. Zederone, a sesquiterpene from Curcuma elata Roxb, is hepatotoxic in mice. *Int J Toxicol*. 2013;32(6):454–462. doi:10.1177/1091581813504595
23. Pintatum A, Maneerat W, Logie E, et al. In vitro anti-inflammatory, anti-oxidant, and cytotoxic activities of four Curcuma species and the isolation of compounds from Curcuma aromatica Rhizome. *Biomolecules*. 2020;10(5):799. doi:10.3390/biom10050799
24. Liu YN, Hu MT, Qian J, et al. Characterization of the chemical constituents of Jie-Geng-Tang and the metabolites in the serums and lungs of mice after oral administration by LC-Q-TOF-MS. *Chin J Nat Med*. 2021;19(4):284–294. doi:10.1016/S1875-5364(21)60028-6
25. Xu T, Li S, Sun Y, et al. Systematically characterize the absorbed effective substances of Wutou Decoction and their metabolic pathways in rat plasma using UHPLC-Q-TOF-MS combined with a target network pharmacological analysis. *J Pharm Biomed Anal*. 2017;141:95–107. doi:10.1016/j.jpba.2017.04.012
26. Wang C-Z, Kim KE, Du G-J, et al. Ultra-performance liquid chromatography and time-of-flight mass spectrometry analysis of ginsenoside metabolites in human plasma. *Am J Chin Med*. 2011;39(6):1161–1171. doi:10.1142/S0192415X11009470
27. Wan JY, Liu P, Wang HY, et al. Biotransformation and metabolic profile of American ginseng saponins with human intestinal microflora by liquid chromatography quadrupole time-of-flight mass spectrometry. *J Chromatogr A*. 2013;1286:83–92. doi:10.1016/j.chroma.2013.02.053
28. Yang C, Qian C, Zheng W, et al. Ginsenoside Rh2 enhances immune surveillance of natural killer (NK) cells via inhibition of ERp5 in breast cancer. *Phytomedicine*. 2024;123:155180. doi:10.1016/j.phymed.2023.155180
29. Kawata Y, Hattori M, Akao T, et al. Formation of nitrogen-containing metabolites from geniposide and gardenoside by human intestinal bacteria. *Planta Med*. 1991;57(6):536–542. doi:10.1055/s-2006-960201
30. Li Y, Pan H, Li X, et al. Role of intestinal microbiota-mediated genipin dialdehyde intermediate formation in geniposide-induced hepatotoxicity in rats. *Toxicol Appl Pharmacol*. 2019;377:114624. doi:10.1016/j.taap.2019.114624
31. Kim BR, Jeong YA, Na YJ, et al. Genipin suppresses colorectal cancer cells by inhibiting the Sonic Hedgehog pathway. *Oncotarget*. 2017;8 (60):101952–101964. doi:10.18632/oncotarget.21882
32. Shenvi S, Diwakar L, Reddy GC. Nitro derivatives of naturally occurring β -Asarone and their anticancer activity. *Int J Med Chem*. 2014;2014:835485. doi:10.1155/2014/835485
33. Johnson SC, Dahl J, Shih TL, et al. Synthesis and evaluation of 3-modified 1D-myo-inositols as inhibitors and substrates of phosphatidylinositol synthase and inhibitors of myo-inositol uptake by cells. *J Med Chem*. 1993;36(23):3628–3635. doi:10.1021/jm00075a018
34. Opitz SE, Mix A, Winde IB, et al. Desulfation followed by sulfation: metabolism of Benzylglucosinolate in Athalia rosae (Hymenoptera: tenthredinidae). *Chembiochem*. 2011;12(8):1252–1257. doi:10.1002/cbic.201100053
35. El-Sayed Ebead E, Aboelnaga A, Nassar E, et al. Ultrasonic-induced synthesis of novel diverse arylidenes via Knoevenagel condensation reaction. Antitumor, QSAR, docking and DFT assessment. *RSC Adv*. 2023;13(42):29749–29767. doi:10.1039/D3RA05799B
36. Di Benedetto C, Borini Etichetti C, Cocordano N, et al. The p53 tumor suppressor regulates AKR1B1 expression, a metastasis-promoting gene in breast cancer. *Front Mol Biosci*. 2023;10:1145279. doi:10.3389/fmolb.2023.1145279
37. Shropshire DB, Acosta FM, Fang K, et al. Association of adenosine signaling gene signature with estrogen receptor-positive breast and prostate cancer bone metastasis. *Front Med Lausanne*. 2022;9:965429. doi:10.3389/fmed.2022.965429
38. DeSantis CE, Fedewa SA, Goding Sauer A, et al. Breast cancer statistics, 2015: convergence of incidence rates between black and white women. *CA Cancer J Clin*. 2016;66(1):31–42. doi:10.3322/caac.21320
39. Kerbel RS. Reappraising antiangiogenic therapy for breast cancer. *Breast*. 2011;20 Suppl 3(0 3):S56–60. doi:10.1016/S0960-9776(11)70295-8
40. Yang R, Xie Y, Li Q, et al. Ruyiping extract reduces lung metastasis in triple negative breast cancer by regulating macrophage polarization. *Biomed Pharmacother*. 2021;141:111883. doi:10.1016/j.biopha.2021.111883
41. Takemura H, Sakakibara H, Yamazaki S, et al. Breast cancer and flavonoids - a role in prevention. *Curr Pharm Des*. 2013;19(34):6125–6132. doi:10.2174/1381612811319340006
42. Selvakumar P, Badgeley A, Murphy P, et al. Flavonoids and other polyphenols act as epigenetic modifiers in breast cancer. *Nutrients*. 2020;12 (3):761. doi:10.3390/nu12030761
43. Singh B, Sharma RA. Plant terpenes: defense responses, phylogenetic analysis, regulation and clinical applications. *3 Biotech*. 2015;5(2):129–151. doi:10.1007/s13205-014-0220-2
44. Burnouf PA, Roffler SR, Wu CC, et al. Glucuronides: from biological waste to bio-nanomedical applications. *J Control Release*. 2022;349:765–782. doi:10.1016/j.jconrel.2022.07.031
45. Liu X, Wang J, Boyer JA, et al. Histone H3 proline 16 hydroxylation regulates mammalian gene expression. *Nat Genet*. 2022;54(11):1721–1735. doi:10.1038/s41588-022-01212-x
46. Lin Y, Li C, Xiong W, et al. ARSD, a novel ERα downstream target gene, inhibits proliferation and migration of breast cancer cells via activating Hippo/YAP pathway. *Cell Death Dis*. 2021;12(11):1042. doi:10.1038/s41419-021-04338-8